Available online at www.sciencedirect.com

ScienceDirect

Advances in Space Research xxx (xxxx) xxx

ADVANCES IN SPACE RESEARCH (a COSPAR publication)

www.elsevier.com/locate/asr

Demonstration of integrated lunar water extraction and capturing system: overview of results from the LUWEX project

Luca Kiewiet *, Svenja Fälker, Mateo Rejón López, Paul Zabel

German Aerospace Center (DLR), Institute of Space Systems, Robert-Hooke-Str. 7, 28359 Bremen, Germany

Received 14 November 2025; received in revised form 9 January 2026; accepted 13 January 2026

Abstract

Sustainable lunar exploration requires efficient in-situ resource utilisation, particularly for water extraction to enable life support and propellant production. The LUWEX project addressed this need by experimentally demonstrating the functionality of an integrated thermal water extraction and capturing system under simulated lunar polar conditions. In a series of tests in a vacuum chamber, a crucible-based heating system with integrated stirring capability was used to sublimate water from icy regolith simulants (up to 13 kg per run, containing 5 wt% of ice in the simulant material). The vapour was deposited on a cryogenic cold trap before liquefaction. Various operational scenarios were examined, including different simulant types, the use of mechanical stirring, and the introduction of contaminants (e.g. methanol) to evaluate their effects on performance. Key findings show that the end-to-end process is feasible at a multi-kilogram scale in a lunar polar crater-like environment, achieving significant water recovery, with over half of the sample's water recovered, peaking at ~73%. Energy-wise, recovery energy efficiency reached 66.33 g/kWh for the icy glass beads simulant and 22.88 g/kWh for the icy regolith simulant experiments. The resulting average water recovery rate corresponds from 2.06 g/h to up to 7.76 g/h (which corresponds to 0.05–0.19 kg/day) in the best-performing run. These values reflect the energy required to recover water and maintain operational temperatures within a permanently shaded region on the Moon. However, dust generation impaired seal integrity and camera visibility. Trace volatiles, such as methanol, markedly reduced capture efficiency by forming a liquid barrier on the capturing device. Nonetheless, these results demonstrate the viability of large-scale lunar water extraction with an integrated system. Critical challenges such as dust mitigation, vapour capture capacity, and contaminant management remain to be solved. The insights gained are relevant to designing robust ISRU water extraction units for future lunar missions.

Keywords: Lunar in-situ resource utilisation; Water extraction; Icy regolith; Thermal vacuum testing; Cold trap

1. Introduction

In-Situ Resource Utilisation (ISRU) is critical for sustainable space exploration, as it enables future missions to reduce reliance on Earth-based resupply. Among the various resources available beyond Earth, water is particularly critical due to its multifunctional role. It supports human life, enables plant cultivation, and can be split via electrolysis to generate hydrogen and oxygen as propellant and energy storage.

Multiple missions have indicated the presence of water at the Moon's poles in a range of concentrations and physical states (see also, Reiss (2024). Neutron spectroscopy measurements show polar hydrogen enrichments consistent with water-equivalent hydrogen in the near-surface regolith, with typical values up to ~0–0.5 wt% at the instrument footprint and earlier Lunar Prospector modelling

* Corresponding author.
E-mail addresses: luca.kiewiet@dlr.de (L. Kiewiet), svenja.faelker@dlr.de (S. Fälker), mateo.rejonlopez@dlr.de (M.R. López), paul.zabel@dlr.de (P. Zabel).

https://doi.org/10.1016/j.asr.2026.01.041
0273-1177/

Please cite this article as: L. Kiewiet, S. Fälker, M. R. López et al., Demonstration of integrated lunar water extraction and capturing system: overview of results from the LUWEX project, Advances in Space Research, https://doi.org/10.1016/j.asr.2026.01.041

suggesting locally higher concentrations (Elphic et al., 2007; Feldman et al., 1998; Sanin et al., 2017). Near-infrared (NIR) and ultraviolet (UV) reflectance observations have also identified surficial or exposed ice/frost signatures in some permanently shadowed regions (PSRs), including "dirty ice" in ice-positive pixels and UV-bright, ultra-cold surfaces consistent with thin surface frost (Gladstone et al., 2012; Hayne et al., 2015; Li et al., 2018). In addition, the LCROSS impact experiment at Cabeus crater detected 5.6 ± 2.9 wt% H_2O in the ejecta plume, alongside other volatiles (Colaprete et al., 2010; Gladstone et al., 2010). Overall, these findings indicate that lunar water is present in multiple forms. On sunlit portions of the Moon, OH/H_2O is adsorbed at low concentrations (on the order of a few hundred ppm), whereas in cold, permanently shadowed areas, water is cold-trapped as ice, potentially with local concentrations reaching tens of wt. % in some observations. The exact physical state of lunar water (adsorbed versus ice) varies with location and depth (Clark, 2009; Hayne et al., 2021; Pieters et al., 2009; Sunshine et al., 2009). The confirmed presence of water ice in polar PSRs makes the Moon an ideal target for ISRU technologies and mission architectures focused on in-situ water utilisation (Ikeya et al., 2025; Kleinhenz and Paz, 2020; Kornuta et al., 2019).

Despite the growing interest and numerous laboratory demonstrations in lunar water ISRU, most published studies to date have tested individual process steps (such as extraction or capture in isolation) at small scales (gram to sub-kilogram quantities). Fully integrated, pilot-scale experiments that combine extraction, vapour transport, and capture under realistic thermal-vacuum conditions are still scarce (Kiewiet et al., 2025). Consequently, experimental validation of integrated water extraction and capture systems at multi-kilogram scales and high-fidelity environmental conditions remains a critical missing step in advancing lunar water ISRU technology readiness.

To address this gap, the LUWEX project (Validation of Lunar Water Extraction and Purification Technologies for In-Situ Propellant and Consumables Production) was launched as an EU-funded initiative to develop and experimentally validate a complete thermal water extraction and purification system under simulated lunar conditions. The project encompasses three primary subsystems: a thermal extraction subsystem, a water capture subsystem, and a downstream water purification subsystem (including quality monitoring). Fig. 1 illustrates the full scope of LUWEX, with the portion addressed in this paper highlighted in red. The overarching objective is to raise the Technology Readiness Level (TRL) of these technologies to 4, laying the groundwork for a future in-situ demonstration mission. Although formally targeting TRL 4, the testing was conducted with integrated hardware in a high-fidelity environment, approaching the conditions expected of TRL 5.

This paper focuses on the experimental validation of the LUWEX thermal extraction and capture subsystems. All experiments were conducted inside a Dusty Thermal Vacuum Chamber (DTVAC) using an integrated setup consisting of a crucible-based thermal extraction system coupled to a cold trap for water-vapour capture and a downstream liquefaction unit. Each test processed a multi-kilogram sample (up to 13 kg of icy material per run), far larger than the sample masses used in most previous studies. The campaign spanned multiple configurations, including tests with both icy lunar regolith simulant and icy glass bead simulant, and examined operational variations such as active sample stirring and the introduction of contaminants (e.g., methanol and fine dust particles). The details of the icy regolith simulant formulation and production are provided in Wache et al. (2025). Downstream purification and water-quality characterisation are part of the broader LUWEX project but are outside the scope of this high-level results paper. Results of these subsystems can be found in Boscheri et al. (2025).

The primary goal of this experimental campaign was to demonstrate the feasibility of a fully integrated thermal extraction and water capture process at a significantly larger scale than prior studies (processing up to 13 kg of simulant per run). Secondary objectives included assessing the effect of sample stirring on water release, evaluating the system's sensitivity to contaminants, and attempting an initial purification by selectively cold-trapping water ice. Additionally, water recovery efficiencies were measured for each test to inform the design of future lunar water extraction missions.

2. Experiment setup

2.1. Experiment environment

The LUWEX experiments were conducted in a dedicated DTVAC, known as the L-Chamber (Kreuzig et al., 2021), specifically designed for cometary physics experiments, but also capable of simulating lunar surface conditions closely resembling those found in PSRs. The chamber itself has an approximate footprint of 1 m × 1 m and a height of about 2 m, providing space to accommodate the experimental hardware and instrumentation, as well as the cooling system, which is further detailed in Table 1.

Inside the L-Chamber, the LUWEX experimental hardware was enclosed within an actively cooled environment, referred to as the cooling shield or cold shroud, made of pillow plates continuously cooled by liquid nitrogen (LN_2). This shroud encompasses the top, side walls, and a large cooling surface at the bottom, ensuring uniform cryogenic conditions representative of the lunar polar environment. The internal volume defined by this cooling shield represents the effective simulated lunar environment, critical for controlling the radiative boundary conditions of the experiment, as can be seen in Fig. 2.

The LUWEX setup effectively formed a vacuum chamber within the main vacuum chamber, with the capability to isolate or interconnect the internal volumes via valve systems. During typical operation, pressures inside the

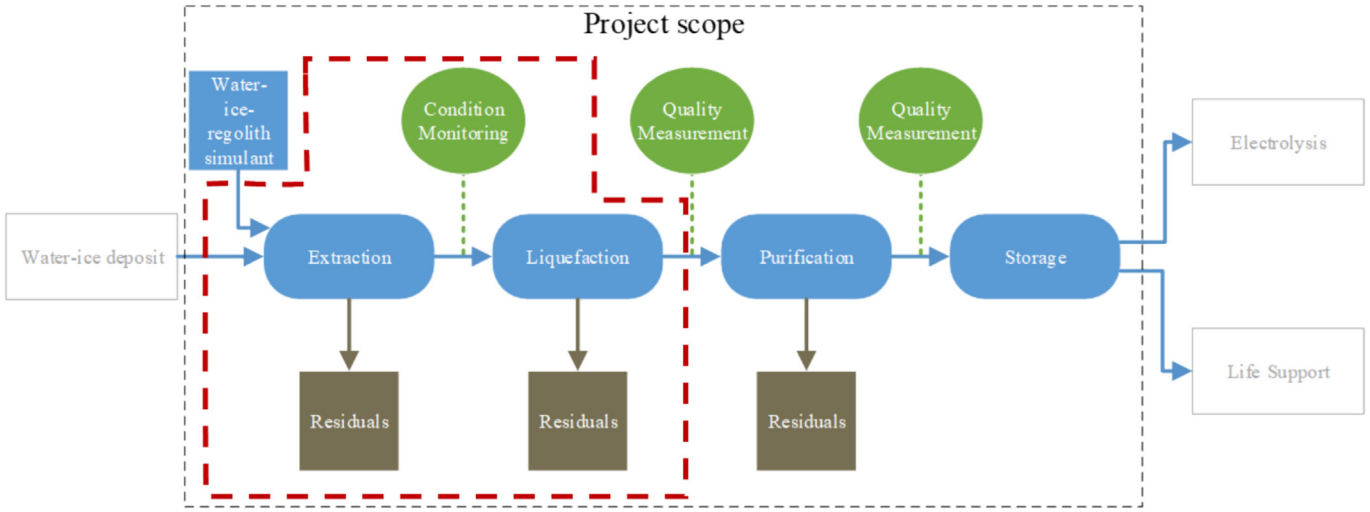

Fig. 1. LUWEX project scope (Imhof et al., 2024) and the scope of this work is superimposed in red.

Table 1
DTVAC parameters and instrumentation.

Parameter	Value/Description
DTVAC inside dimensions	1530 × 700 × 700 mm^3
Cold shroud type	LN_2-cooled pillow plates
Cooling surfaces	Top, sides, and bottom plate
LN_2 coolant temperature	~-170 °C
LUWEX system pressure during operation	~10^{-3} mbar
Chamber pressure (outside LUWEX)	~10^{-5} mbar
Main pump	Turbo-molecular pump
Backing pump	Dry multi-stage roots pump

LUWEX system were maintained between 10^{-3} mbar and 10^{-1} mbar, allowing for ice sublimation, while the surrounding chamber volume reached significantly lower pressures of approximately 10^{-5} mbar. This pressure regime ensured minimal convective heat transfer and prevented gas conduction between the experimental hardware and the cooling surfaces, replicating the vacuum environment encountered on the lunar surface.

The chamber was equipped with multiple pumps, including a turbomolecular pump for achieving deep vacuum levels and a backing (roughing) pump for initial evacuation (see Table 1). Temperature measurements were predominantly carried out using platinum resistance thermometers (primarily Pt-1000 sensors). Pressure monitoring utilised multiple gauge types designed to operate accurately across the entire relevant vacuum range from above 1 mbar down to 10^{-8} mbar. Additionally, cameras were installed at the cold trap and liquefaction chamber to visually monitor the capturing and delamination process, which is further explained in Section 3.2.

2.2. Simulant materials

Two types of icy simulants were used in the LUWEX experiments to act as the icy regolith, namely, icy regolith simulant and icy glass beads. The glass beads were utilised to prevent issues arising from dust mobilisation. In Fig. 3 an overview of the materials is presented.

2.2.1. Regolith simulant

The regolith simulant was provided by Lunex GmbH (Berlin, Germany). This simulant is composed of a mixture consisting of 75% anorthosite (TUBS-T) and 25% basalt (LX-M). The rationale behind this mixture was to achieve a realistic representation of the lunar surface materials relevant for water extraction studies, taking into account particle size distribution, mineralogy, and geotechnical properties of the lunar south polar region. It has a granular form with highly angular particles, resulting in a bulk density of 1.24 g/cm^3 with a particle size distribution in the range of <0.01–1 mm. The detailed mineralogical and chemical composition of the regolith simulant is described in Tables 2 and 3.

Specific physical properties of the LX-M simulant, such as particle size distribution, have been previously characterised in Patzwald et al. (2025b) and Patzwald et al. (2025a). Data about the TUBS-T simulant can be found in Linke et al. (2020).

2.2.2. Ice particles

Micrometre-scale ice particles were generated using a proven method, as described in Kreuzig et al. (2023). A piezoelectric nozzle atomised distilled water into fine droplets, which froze rapidly while falling through a channel cooled by liquid nitrogen. This process produced small, spherical ice particles, with a mean radius of 2.4 ± 0.1 µm, which were collected in a liquid nitrogen bath and subsequently dried under vacuum to remove residual nitrogen. The resulting ice particles maintained their distinct granular form, enabling homogeneous mixing with simulant material without clumping. The baseline percentage of ice inside the simulant material (glass beads or regolith simulant) was 5 percent by weight, following the LCROSS impact plume mission results.

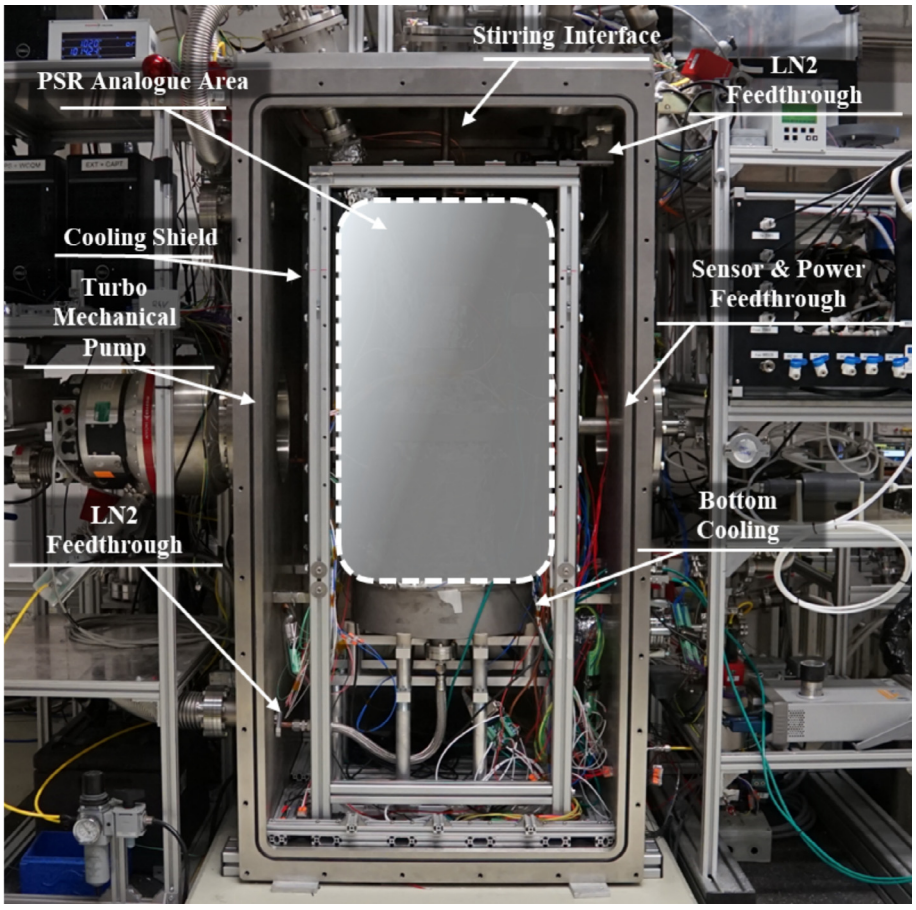

Fig. 2. The DTVAC and its systems.

Fig. 3. Simulants used in the LUWEX project. A) LUNEX Regolith simulant, B) Ice particles, C) Glass beads, and D) the mixed Icy Regolith simulant.

In selected experiments, methanol was deliberately introduced into the icy simulant to represent realistic contamination based on observed lunar volatile compositions. Specifically, methanol was included at approximately 1 wt % in the icy simulant to reflect its abundance as detected by the LCROSS mission under worst-case conditions (Colaprete et al., 2010; Gladstone et al., 2010; Holquist et al., 2021), in which methanol was detected at concentrations up to 0.67 mol% relative to water vapour, corresponding to approximately 11.9 g/L based on updated

Table 2
Regolith simulant chemical composition as oxide sum (Lunex Technologies GmbH, 2024).

Component	Weight %
SiO_2	48.7
TiO_2	0.7
Al_2O_3	26.1
FeO	3.3
MgO	2.6
CaO	13.0
Na_2O	3.2
K_2O	0.6
MnO	0.1
Cr_2O_3	<0.1
P_2O_5	0.1

Table 3
Regolith simulant mineral composition (Lunex Technologies GmbH, 2024).

Mineral phase	Volume %
Plagioclase feldspar (Labradorite)	9.6
Plagioclase feldspar (Bytownite)	72.75
Pyroxene (Augite)	10.48
Olivine (Forsterite)	4.6
Titanomagnetite	0.25
Alkali Feldspar	0.08

post-mission analyses. The methanol was added to the liquid water before creating the ice particles, meaning the water–ice and the methanol were intimately mixed.

The concentration of methanol used was within established safety limits for both the DTVAC hardware and personnel. While numerous other volatile compounds were detected during the LCROSS impact experiment, these were not introduced in the LUWEX water extraction and capturing experiments due to operational and safety constraints. Methanol was selected because its phase diagram closely resembles that of water, making it likely the most challenging contaminant to actively separate during cold-trap capturing (Holquist et al., 2020), and thus the best proxy to test the sensitivity to other volatiles of the LUWEX water extraction and capturing hardware.

2.2.3. Glass beads

Uniform glass beads (approx. 1 mm in diameter) were used to simplify early experiments by eliminating dust mobilisation issues. These beads are composed primarily of silica and have well-defined, consistent dimensions, facilitating clearer interpretation of system behaviours such as heating distribution, vapour transport, and capturing efficiency. Supplier details and specific material properties can be found in Sigmund Lindner GmbH (2018).

2.3. LUWEX water extraction and capturing design

The LUWEX Water Extraction and Capturing System (WECS) comprises two main integrated subsystems: the Water Extraction Subsystem (WES) and the Water Capturing and Liquefaction Subsystem (WCS). These subsystems were designed for and tested within the DTVAC to replicate lunar conditions closely. This section describes the hardware components (shown in Fig. 4) and their configuration, while detailed operational procedures are covered in Section 3.2.

2.3.1. Water extraction subsystem

The main function of the WES is to heat the icy simulant until sublimation occurs and let the resulting water vapour travel to the WCS. The central element of the extraction subsystem is a cylindrical, stainless-steel crucible specifically designed for containing icy regolith simulants or glass beads. This crucible features 8 internal cartridge heaters and externally wrapped heating wires, allowing for controlled and uniform heating up to approximately 60 °C. The internal cartridge heaters directly heat the icy simulant sample, whereas the externally wrapped heating wires control the temperature of the chamber walls to prevent unwanted frost from forming. To further enhance heat distribution and thermal efficiency, a mechanical stirring mechanism driven by an external motor is integrated directly within the crucible, on which all cartridge heaters are mounted. The design of the WES is inspired by Purrington et al. (2023) for agitating the sample to increase the thermal diffusivity, and by Reiss et al. (2019) for the wall heating method. A secondary objective of this experiment was to investigate the efficiency increase of stirring the sample versus static heating, and thereby evaluating its usefulness. Heating wires with a defined resistance per meter were wrapped around all surfaces of the extraction subsystem, including the crucible walls and the vapour transfer tube, thereby preventing the unintended deposition of water vapour on colder surfaces when travelling towards the capturing subsystem.

2.3.2. Water capturing and liquefaction subsystem

The water capturing subsystem is centred around two conical copper cold fingers actively cooled internally with liquid nitrogen to approximately −170 °C. These cold fingers act as primary deposition surfaces for sublimated water vapour coming from the WES. To ensure deposition occurs solely on the designated cold fingers, external heating wires were applied to all surrounding surfaces of the capturing chamber, maintaining them between 0 and 20 °C and preventing unintended frost accumulation. The design of the cold traps was inspired by Holquist et al. (2021). A secondary objective of these cold fingers was to enable the precise control of the surface capturing (deposition) temperature so that only water–ice is captured, leaving other volatiles as a gas and thereby performing a first step of purification.

Ice deposited on the cold fingers can be periodically delaminated through brief heating of the cold fingers, similarly to what is done in Jurado et al. (2021). A pneumatically actuated slider valve is installed between the capturing cham-

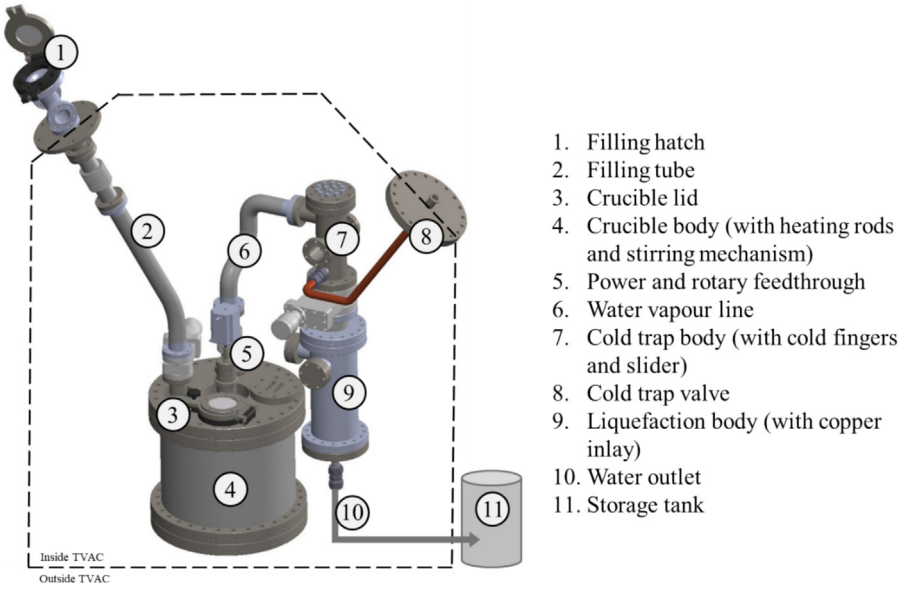

Fig. 4. LUWEX WECS components.

ber and the liquefaction chamber to isolate the liquefaction chamber for subsequent melting of accumulated ice.

2.3.3. Hardware specifications

Table 4 provides detailed specifications of each subsystem component, including physical dimensions, heater types, power ratings, and relevant notes regarding their positioning and function. All heaters not listed as WES or WCS were still added for later energy calculations on total recovery.

Fig. 5 shows an overview of the fully assembled LUWEX system inside the DTVAC, illustrating component arrangement, insulation placement, and visible hardware details. Fig. 6 presents a detailed 3D schematic model indicating the precise placement of heating elements, sensor locations, valve locations and the stirring mechanism, providing a comprehensive view of the integrated hardware design. Cartridge heater power and its integrated temperature sensor data were transmitted through a slip ring integrated inside the crucible lid.

The inner volume of the WECS could be evacuated through the valve at the cold trap and through another valve connected to the filling hatch, though the latter was not utilised during experiments.

The LUWEX system was operated through a control and data acquisition interface. Heating sequences, the stir-

Table 4
Hardware dimensions and heater power.

Component	Dimensions (mm)	Type	Resistance (Ω)	Power (W)	Voltage (V)	Notes
Crucible body (WES)	Ø 300 × H 300	Heating Wire	9.3	247	48	30 m cable, 0.3 Ω/m
Crucible lid (WES)	Ø 300 × 20	Heating Wire	25	92	48	5 m cable, 5 Ω/m
Stirring rods (WES)	Heaters: Ø 8 × 100 Rods: Ø 12 × 150	Cartridge Heaters	–	800	–	8 rods, embedded in the stirring frame
Vapour tube (WCS)	L 400 × Ø 40	Heating Wire	26.7	86	48	4.1 m cable, 5 Ω/m
Filling tube	L 600 × Ø 40	Heating Wire	20.5	112	48	6 m cable, 3.4 Ω/m
Cold trap body (WCS)	Ø 66 × H 210	Heating Wire	15.6	147	48	3.5 m cable, 5 Ω/m
Cold fingers	L 170 × Ø 26–14	LN_2 cooled	–	–	–	Cooled to ~ -170 °C
Cold fingers (heating) (WCS)	–	Heating Wire	4.5 / 4.4	128	24	0.95 m each, 5 Ω/m
Liquefaction chamber (WCS)	Ø 100 × H 270	Heating Wire	13.4	171	48	4 m cable, 3.4 Ω/m
Liquefaction copper inlay (WCS)	Ø 75 × H 180	Heating Wire	9.8	235	48	2.75 m cable, 3.4 Ω/m
Water outlet tube (WCS)	L 400 × Ø 16	Heating Wire	20.4	113	48	4 m cable, 5 Ω/m
Slider valve	Ø 66	Pneumatic	–	–	–	–

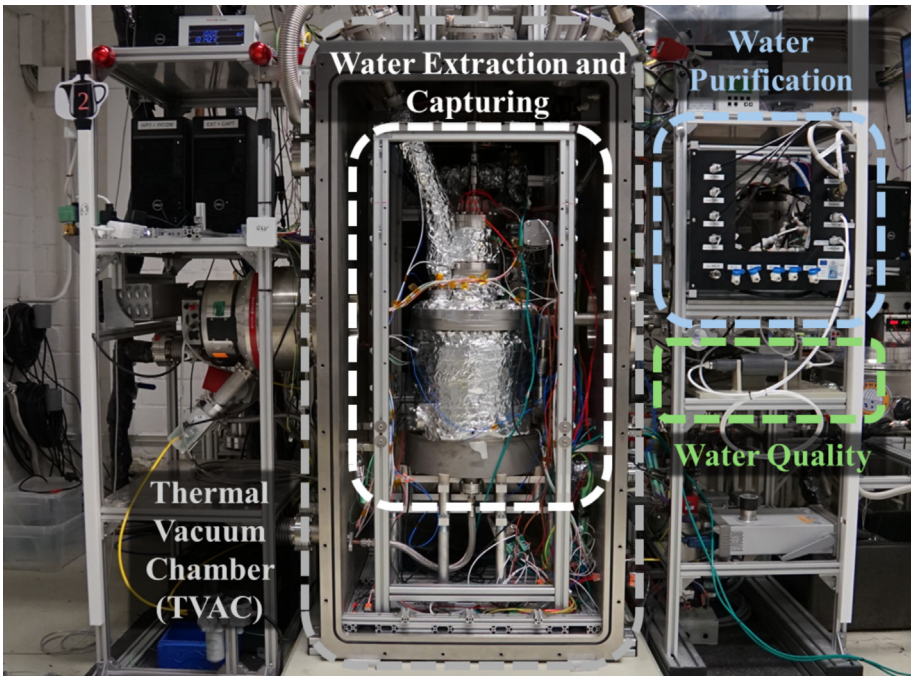

Fig. 5. The integrated Water Extraction and Capturing system inside the DTVAC, and Water Purification and Quality systems next to it.

ring mechanism, and (slider) valve operations could be executed through this software. All sensor data, including temperatures and pressures, were continuously logged at a sampling rate of 1 Hz using National Instruments hardware modules and LabVIEW software. Images captured during critical phases (capturing and delamination) were recorded independently for subsequent analysis. Detailed specifications of the sensors and instrumentation are summarised in Table 5.

3. Methodology

The experiments were structured into a single, integrated campaign with multiple distinct test attempts designed to validate the end-to-end water extraction, capturing, and liquefaction process under simulated lunar conditions. The campaign involved three preliminary attempts, during which technical issues, primarily related to heating element failures, dust issues, and system repairs, prevented full completion of the experiments. After resolving these issues, the first successful experiments were conducted using glass beads as a substitute for regolith simulant to avoid complications arising from dust mobilisation within the vacuum chamber, thereby allowing the functionality of the subsystems to be tested.

The tests began by filling the crucible with icy simulant and sequentially executing all the phases, from extraction until eventual liquefaction. Subsequent tests adopted a cumulative approach, refilling fresh icy simulant directly onto the previously processed dried simulant. Each refill was carefully calculated to maintain an approximate total ice mass fraction of 5%. Experiments were conducted up to a total of 13 kg of icy simulant (glass beads or regolith simulant).

All experiments were executed in a fully integrated manner, utilising the complete system assembled within the DTVAC. To support transparency and comparability with other lunar water extraction experiments, key performance metrics are reported following the standardised framework proposed in the authors' review on lunar water extraction (Kiewiet et al., 2025). Masses of input material, extracted water, and residue were weighed after each experiment. Heater duty cycles and power were logged to calculate energy input. This data is used in Chapter 4 to report metrics such as recovery efficiency and energy-specific performance. All data logging devices are listed in Table 5.

3.1. Sample and environment preparation

Before all experiments, the sample material had been dried out for 12 h at 110 °C, following National Aeronautics and Space Administration [NASA] (2021) practices. Samples were prepared by then placing either the dried-out glass beads or regolith simulant in a sealed stainless-steel storage tube to prevent atmospheric humidity from entering the sample. The tube was then submerged in a metal pot filled with liquid nitrogen, itself housed within a large Styrofoam insulating box. The liquid nitrogen bath was replenished overnight, ensuring the sample maintained cryogenic temperatures for at least 12 h and until ready for mixing. The equipment used for this can be seen in Fig. 7.

The ice component added to the simulant was produced through a method that generated fine, micrometre-sized ice particles (Kreuzig et al., 2023). These ice particles were

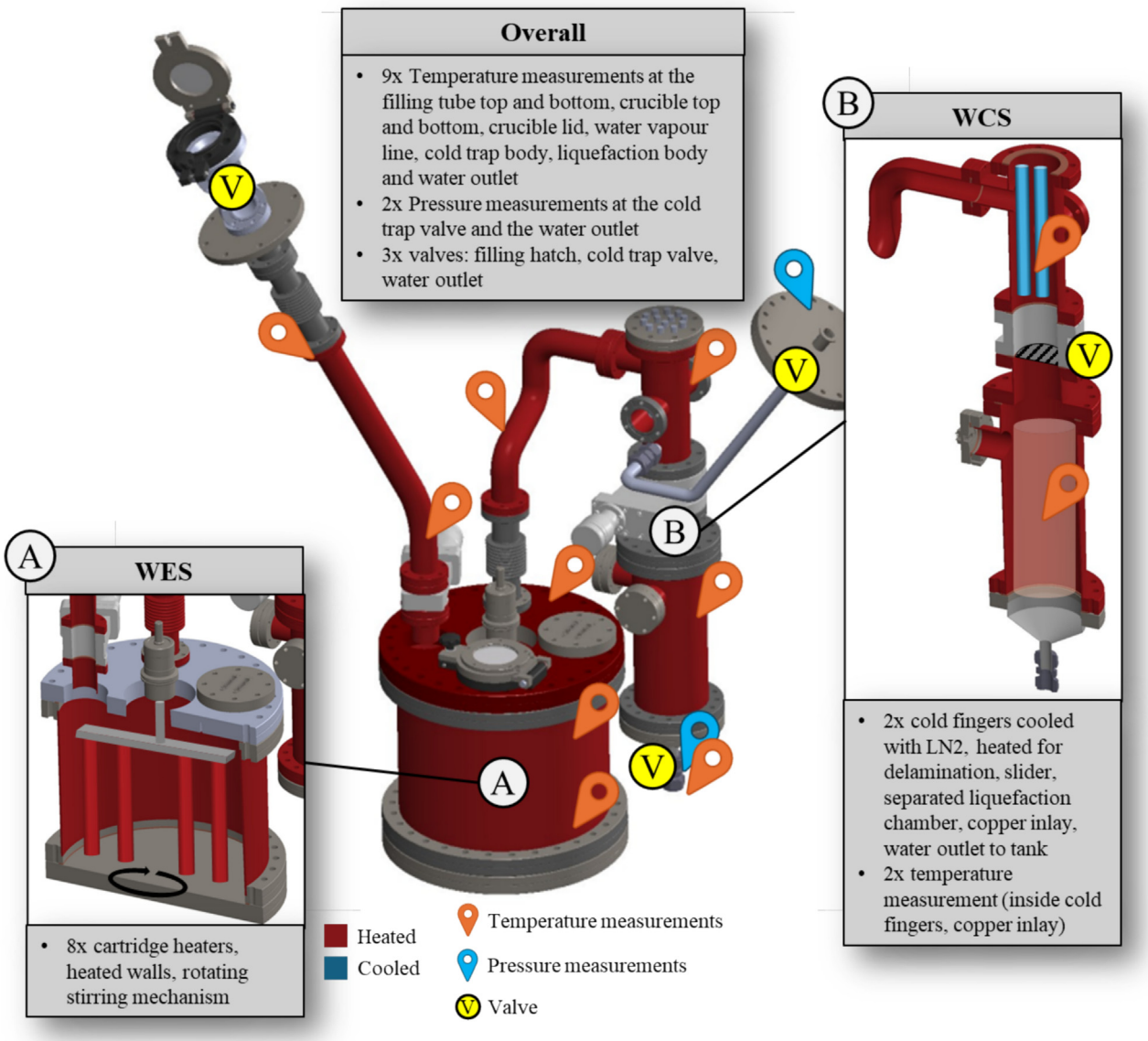

Fig. 6. 3D schematic of the water extraction and capturing subsystems showing the placement of all heaters and cooling devices, and all sensors.

incrementally added and manually stirred into the pre-cooled regolith or glass beads within the cooled Styrofoam box until the ice reached 5 wt%. The homogeneity of the ice-regolith mixture was periodically checked by extracting small subsamples, which were then dried and weighed to verify the consistent distribution of ice.

Once the icy simulant mixture was prepared, it was introduced into the system through a dedicated filling tube connected directly to the crucible. Before opening this tube, the crucible's internal environment was pressurised with argon gas, due to its density and inert characteristics, to prevent atmospheric frost formation and maintain the integrity of the cryogenic conditions. The icy simulant was manually transferred through the filling tube into the crucible. After filling, the system was immediately sealed and gradually evacuated to a pressure level of roughly 10^{-2}–10^{-3} mbar until it stabilises before commencing the extraction process.

3.2. Concept of operations

A visual operational concept with all the phases is presented in Fig. 8. A typical experiment began with the crucible filled with icy simulant and the system stabilised at low vacuum and cryogenic temperatures representative of lunar PSRs. Before heating, liquid nitrogen was circulated through the copper cold fingers within the capturing subsystem, cooling them internally to approximately −170 °C. The surrounding surfaces of the capturing chamber were kept relatively warmer (0–20 °C) to prevent unintended frost accumulation, thus ensuring precise control over ice deposition. This also causes the cold finger outer

Table 5
Sensors and measurement equipment types.

Measurement type	Instrumentation	Model / Type	Quantity	Accuracy	Notes
Temperature	RTDs Pt-1000		40	± (0.1 + 0.0017|t|) °C *	All subsystems.
Temperature	RTDs Pt-100		4	± (0.3 + 0.005 | t |) °C *	Cartridge heater sensors.
Pressure	High vacuum gauge	Pfeiffer PKR 251	1	±30% (10^{-8}–10^{-2} mbar)	For deep vacuum.
Pressure	Low vacuum gauge	Pfeiffer TPR 280	1	±15% (10^{-3}–10^{2} mbar)	For above 1 mbar.
Mass	Precision balance	Kern 572-33	1	±0.01 g	Weighing water and residual material.
Mass	Precision balance	Ranger 300 R31P15	1	±0.5 g	Weighing simulant and residual material.
Image	Camera	Daheng MER-1520-7GC	2	4608 × 3288px	Image logged every 15 sec.
Control & data acquisition	Software/Hardware	LabVIEW, NI-9425, NI-9375, NI-9226, NI-9220	–	Sampling rate: 1 Hz	Sensor integration, logging, and control.

* t is the temperature in °C.

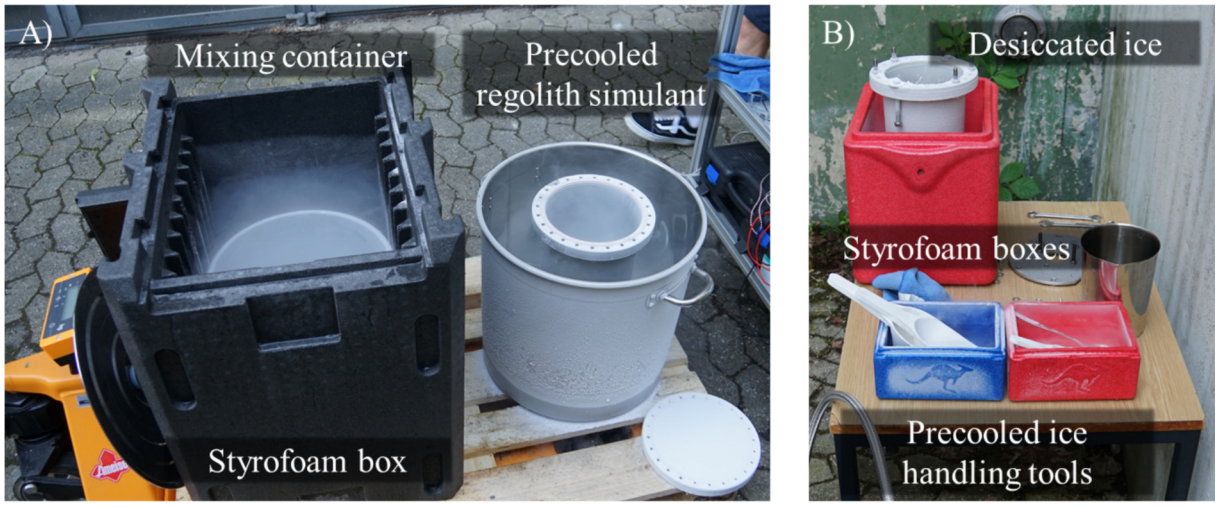

Fig. 7. Icy simulant preparation equipment. A) The large Styrofoam box with the mixing container in it, and the precooled simulant container in a pot surrounded with liquid nitrogen. B) The container for the ice particles and the boxes for precooling tools.

surface to heat up due to the thermal radiation of the capturing chamber, adding uncertainties to the surface temperature of the cold fingers, meaning the cooling had to constantly account for this.

Extraction was initiated by heating the simulant through cartridge heaters embedded within the crucible, operating on a controlled duty cycle (e.g., 10 s ON, 50 s OFF) and a set temperature to manage thermal load and heater safety. Concurrent mechanical stirring was applied to selected experiments to attempt to improve thermal homogeneity and enhance sublimation efficiency. As the simulant temperature increased, sublimated water vapour travelled towards the capturing subsystem, where it deposited onto the outer surface of the actively cooled copper cold fingers. The capturing and deposition process was observed via a camera looking through a viewing port with a view of the cold fingers.

The capturing process was operated concurrently with extraction, capturing sublimated vapour until a stable low-pressure state was reached, indicating that sublimation had effectively ceased, or when the cold fingers were deemed full of ice. Afterwards, the extraction process was stopped by deactivating the heating rods inside the crucible. Once the vapour pressure stabilised, the delamination phase was initiated by heating the cold fingers, causing accumulated ice deposits to detach and fall into the liquefaction chamber beneath, as confirmed through internal camera monitoring.

If the icy sample was not yet fully desiccated, the process would start again with another extraction-capturing-delamination (ECD) run, as visualised in the flow diagram in Fig. 9. If the crucible was refilled with icy simulant on top of the already desiccated material, the process likewise restarted but constituted a new test number. Following the delamination phase, the liquefaction chamber, which could be sealed via a dedicated slider mechanism, was typically closed only at the conclusion of the overall experimental run, rather than after each ECD run. After closure, accumulated ice was warmed to induce melting, thus completing the liquefaction step and recovering liquid water from the storage tank. Ultimately, either the crucible would be full (but desiccated), or the liquefaction chamber would be observed through the cameras to be full of ice. Then, the liquefaction process would be started: either the lique-

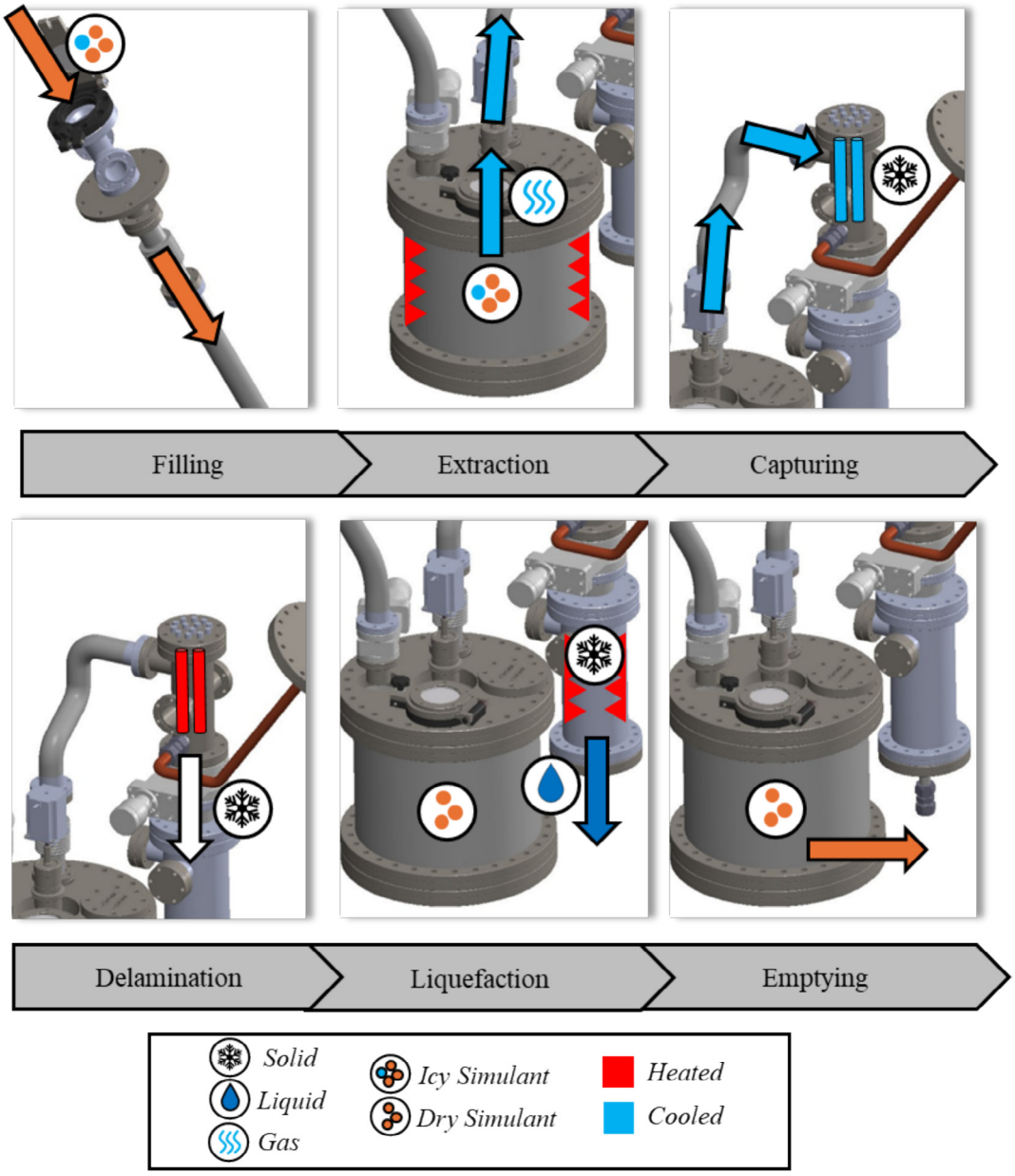

Fig. 8. Operational concept of the water extraction, capturing, and liquefaction process, as well as filling and emptying.

faction heaters are started, or the cooling system is turned off, and the entire experiment setup is allowed to warm up, which would liquefy the ice and cause it to flow to the storage chamber outside of the DTVAC (in a lunar implementation, liquid handling would require a sealed/controlled reservoir, otherwise storage as ice is the likely default). After this, the experiment is concluded.

3.3. Post-experiment steps

At the end of each experiment, following liquefaction, the vacuum chamber was opened to reset the system. Liquid water obtained from the liquefaction phase was taken out of the storage tank and weighed.

To enable efficient reuse of the crucible between experimental runs, a dedicated emptying method was implemented. The crucible featured an outlet near the bottom edge connected externally through a tube, allowing regolith removal via a high-powered vacuum cleaner. During operation, the stirring mechanism, equipped with an off-centre beam, directed the regolith towards this outlet. To maintain continuous airflow and effective extraction, the filling tube was opened as an air inlet during emptying.

This approach was successfully tested using regolith simulant. However, concerns over potential damage to equipment prevented its regular use during subsequent experiments involving glass beads. Ultimately, the preferred

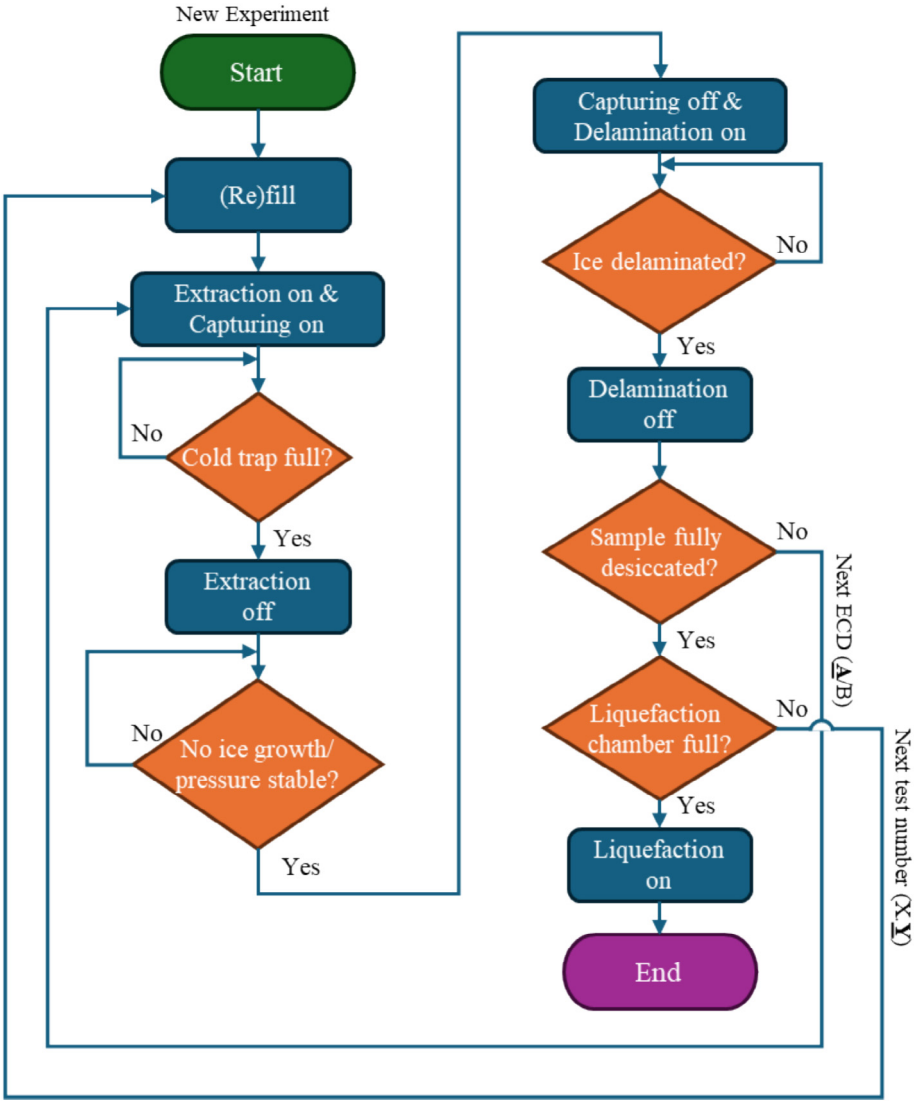

Fig. 9. Flowchart of the different phases during the experiment.

method during most runs became manual removal with a dedicated hoover. So, after the experiments, the crucible was opened entirely, the remaining material was emptied, quickly weighed, oven-dried for 12 h at 110 °C (NASA, 2021), and re-weighed to determine the residual water content accurately. The crucible's design, particularly the stirring mechanism, significantly facilitated this manual emptying process. Although effective for experimental purposes on Earth, the vacuum-based emptying mechanism does not directly translate into lunar conditions, where alternative removal methods would be required.

This procedure enabled the precise determination of total sublimated water, residual water content, and captured water mass, enabling a calculation of losses to both the vacuum system and internal surfaces. This detailed accounting allowed accurate calculation of capturing efficiency and identification of systematic water losses throughout the integrated extraction and capturing process, as specified in the next section.

3.4. Performance metrics and calculations

The experimental performance was evaluated using several key metrics, derived from direct measurements and aimed at quantitatively assessing system efficiency, water extraction performance, and capturing effectiveness. These metrics are based on the ones presented in Kiewiet et al. (2025). Each metric calculation is defined below.

3.4.1. Total active time

The total active time (t_{active}) of each experiment is defined as the sum of the capturing phase duration ($t_{capturing}$) and the subsequent delamination duration ($t_{delamination}$) summed across the multiple refills and attempts per experiment:

$$t_{active\_total} = \sum_i \left(t_{capturing,i} + t_{delamination,i}\right) \quad (1)$$

The capturing and extraction phases overlap partially, while delamination occurs sequentially immediately after

capture. This metric represents the relevant duration when actively recovering water.

3.4.2. Total energy used

The total energy used (E_{total}) during each experiment is calculated by summing the energy consumed by each heater. Each heater's energy is determined by multiplying its rated power (P_i) by its total accumulated on-time ($t_{on,i}$):

$$E_{total} = \sum_{i \in \text{heaters}} P_i \cdot t_{on,i} \tag{2}$$

where P_i represents the power consumption of each heater element (crucible, cold trap, liquefaction heaters, filling tube, vapour tube, etc.) and t_i represents their respective operating times.

3.4.3. Total extraction time

The total extraction time ($t_{extraction\_total}$) refers to the sum of all individual extraction phases within a given experiment, including those spanning multiple refill cycles. It represents the cumulative time during which the extraction subsystem was actively operated per experiment.

$$t_{extraction\_total} = \sum_i t_{extraction,i} \tag{3}$$

3.4.4. WES Energy used

WES Energy ($E_{extraction}$) accounts for the cumulative electrical energy consumed by all heaters involved in the WES, including crucible body, crucible lid, and stirring cartridge heaters. This value is used to calculate the extraction energy efficiency and isolates heater consumption specific to sublimating and outgassing the ice from the sample.

$$E_{extraction} = \sum_{i \in \text{WES}} P_i \cdot t_{on,i} \tag{4}$$

3.4.5. Recovery percentage

The recovery percentage quantifies the efficiency of the entire process by comparing the total mass of water recovered ($m_{recovered}$) after liquefaction, to the initial mass of ice present in the sample ($m_{initial}$):

$$\text{Recovery } \% = \frac{m_{recovered}}{m_{initial}} \times 100\% \tag{5}$$

3.4.6. Recovery rate

The recovery rate measures the amount of water recovered per unit time, allowing comparison of system speed across different experimental conditions:

$$\text{Recovery Rate} = \frac{m_{recovered}}{t_{activetotal}} \tag{6}$$

3.4.7. Residual ice mass

Residual ice mass ($m_{residual}$) refers to the quantity of water remaining within the sample after the experiment. This value is measured by immediately weighing the sample after removal, oven-drying it, and then re-weighing to determine the mass difference. The calculation is:

$$m_{residual} = m_{wet\_sample} - m_{dry\_sample} \tag{7}$$

3.4.8. Extracted mass

The extracted mass ($m_{extracted}$) of water vapour is the total mass of water successfully sublimated and removed from the initial ice sample mass:

$$m_{extracted} = m_{initial} - m_{residual} \tag{8}$$

3.4.9. Extraction percentage

The extraction percentage assesses the effectiveness of the sublimation and outgassing process by quantifying the amount of water that successfully leaves the sample. It is computed using the initial and extracted ice masses:

$$\text{Extraction } \% = \frac{m_{extracted}}{m_{initial}} \times 100\% \tag{9}$$

3.4.10. Extraction rate

The extraction rate quantifies the amount of water vapour successfully outgassed (sublimated and removed from the sample) per unit time. It is calculated by dividing the extracted mass by the total extraction time across all cycles:

$$\text{Extraction Rate} = \frac{m_{extracted}}{t_{extraction\_total}} \tag{10}$$

3.4.11. Capturing percentage

The capturing percentage is the ratio of water successfully captured and ultimately recovered from the water vapour extracted from the sample, providing insight into the performance of the capturing subsystem:

$$\text{Capturing } \% = \frac{m_{recovered}}{m_{extracted}} \times 100\% \tag{11}$$

3.4.12. Loss mass

The loss mass (m_{loss}) represents water that was sublimated and removed from the sample but not recovered as liquid. This can be vapour that escaped through pumping or residual deposition on internal surfaces, and is calculated as:

$$m_{loss} = m_{initial} - m_{residual} - m_{recovered} \tag{12}$$

3.4.13. Extraction energy efficiency

The extraction energy efficiency evaluates how much water is recovered per unit of energy input from heaters. For this metric, only the power consumption of heaters directly involved in the water extraction subsystem is considered ($E_{extraction}$), excluding auxiliary subsystem heaters:

$$\text{Extraction Energy Efficiency} = \frac{m_{extracted}}{E_{extracted}} \tag{13}$$

3.4.14. Recovery energy efficiency

This metric reflects the overall energy effectiveness of the full water extraction, capturing, and liquefaction system. It

is calculated by dividing the total mass of recovered liquid water by the total energy consumed by all heaters throughout the experiment:

$$\text{Recovery Energy Efficiency} = \frac{m_{recovered}}{E_{total}} \quad (14)$$

4. Results

4.1. Overview of experiments

This section presents the results from the successful LUWEX experiments. While initial test attempts informed critical operational adjustments, detailed data from these preliminary runs are excluded here for clarity. Instead, the parameters from four primary test campaigns are presented in Table 6, numbered from 1.y to 4.y for clarity. The ''y'' stands for the number of refills that were done during that specific test attempt. The refill sum stands for the amount of material in the crucible after it's been refilled (e.g. to go from 4000 g to 6000 g, 2000 g of material would be added, in which the ice would be mixed to have the overall ice mass percentage be 5). Additionally, some experiments involved multiple ECD runs without a refill, especially when the ice masses increased and the cold trap could not effectively capture the total amount of ice. The ECD run number indicates this, as well as the total number of ECD runs in that specific test number.

Experiment 1 served as the initial successful proof-of-concept test. Glass beads were used as the simulant material to bypass the challenges dealing with the dust, and the primary goal was to confirm successful water extraction, capturing and liquefaction. This experiment consisted of a single refill, resulting in two ECD runs total. The ice fraction was not strictly controlled to be 5% of the total mass and varied after the first refill, but the goal here was to see whether the capturing subsystem worked.

Experiment 2 also utilised glass beads but maintained a consistent 5% ice mass fraction throughout the entire experiment. It was more extensive, reaching a final total mass of 13 kg after three additional refills, each followed by extraction-capturing-delamination runs. In total, five extraction cycles occurred due to the final refill requiring a further cycle to extract all accessible ice effectively.

Experiment 3 investigated the effects of contamination by adding approximately 1% methanol to the water used during ice production. This was done to evaluate how contaminants influence the overall performance of the system, particularly the capturing phase. Initially, the experiment was conducted without stirring. Stirring was later activated partway through the test to observe any changes in sublimation behaviour and to evaluate whether the added complexity of a mechanical stirring system could be justified by improved extraction efficiency. The campaign ended at 8 kg total mass after 2 refills.

The decision to alter two parameters, i.e. methanol contamination and mechanical stirring, during a single experiment was made in response to time constraints and the experience gained from the previous experiments that slower heating was likely better in terms of capturing efficiency and ultimately recovery efficiency. Although this approach limited the ability to attribute observed effects to one specific factor, it allowed for a more effective use of available DTVAC time. The assumption was that the stirring would only affect the extraction rate, whereas methanol would affect the capturing subsystem.

Experiment 4 marked a transition from glass beads to lunar regolith simulant. Unlike previous tests, the full 13 kg of icy regolith simulant was loaded in a single fill. Due to the capturing system bottleneck, four extraction-c

Table 6
Summary of Input Parameters for all conducted successful LUWEX Experiments.

Test number	Type	Simulant mass (g)	Ice mass (g)	Ice percentage (wt.%)	Stirring?	Contaminants?	ECD run no.
1.0	Glass beads	4400	221	4.78	Yes	No	(1/1)
1.1		8800*	221	2.45	Yes	No	(1/1)
2.0	Glass beads	4000	211	5.01	Yes	No	(1/1)
2.1		6000*	316	5.00	Yes	No	(1/1)
2.2		9000*	475	5.01	Yes	No	(1/1)
2.3		13,000*	685	5.01	Yes	No	(1/2) (2/2)
3.0	Glass beads	4000	211	5.01	Partially	CH_3OH 0.85%†	(1/1)
3.1		6000*	316	5.00	Partially	CH_3OH 1%†	(1/1)
3.2		8000*	421	5.00	Partially	CH_3OH 1%†	(1/1)
4.0	Regolith Simulant	13,000	653	4.78	No	Dust particles	(1/4) (2/4) (3/4) (4/4)

* The sum of the simulant mass in the crucible after refilling on top of the desiccated leftover mass.
† CH_3OH mass percentage is relative to ice mass.

apturing-delamination cycles were performed without refills.

While each experiment was conducted independently with unchanged hardware, operational techniques and procedures were incrementally refined based on practical experience gained from preceding tests, resulting in progressively improved operational proficiency. A picture of the recovered water is presented in Fig. 10.

4.2. Recovery and energy metrics

Key performance metrics for each test campaign, including water recovery and energy efficiency, are summarised in Table 7. Precise measurements of input mass, recovered water mass, and residual ice mass allowed calculation of critical metrics such as extraction efficiency (mass of sublimated ice and outgassed vapour per unit energy) and recovery efficiency (mass of recovered water per unit energy). Energy inputs were determined using logged heater duty cycles, resistances, and power data.

The results in Table 7 correlate with operational parameter changes between experiments. In Experiment 1, the residual ice mass was not measured after sample removal, preventing the extraction-related calculations. Nonetheless, a moderate recovery percentage was achieved. This run primarily served to gain operational experience with the system.

Experiment 2, conducted with larger samples and ice masses and improved operational procedures, yielded a slightly higher recovery percentage and a higher recovery rate. The measured residual ice mass was small, indicating a high extraction percentage. With both extracted and recovered masses known, the capture percentage and system losses could be determined, enabling the calculation of extraction and recovery energy efficiencies.

In Experiment 3, stirring was omitted during the first half of each cycle, and methanol was added to the sample. The recovery percentage dropped by approximately 10%, and the recovery rate decreased, consistent with slower heat distribution in the absence of stirring, and an overall relatively longer experiment time per test. The residual ice mass was minimal, indicating high extraction efficiency, but the capturing percentage fell by 16% compared to Experiment 2. This reduction is likely linked to the methanol addition, which inhibited the cold trap's ability to deposit water vapour, as will be discussed in the observations section 0.

Finally, Experiment 4 replaced glass beads with lunar regolith simulant and was performed without stirring, and took more time per ECD run. This resulted in the highest recovery percentage of all tests, but also the lowest recovery rate. Some residual ice remained, giving a slightly reduced extraction percentage, but the capturing percentage of the extracted mass was high (89%). The slower process improved cold trap performance, reducing system losses. Extraction and recovery energy efficiencies were, however, significantly lower than in the glass bead tests, likely due to differences in the thermal properties of the regolith simulant and the slower recovery rate, meaning the system had to keep itself operational for longer and thus consumed overall more energy.

The reported recovery energy efficiency values account for the total energy required to operate the system within a PSR environment. This includes not only the energy for sublimation and capturing, but also the additional heating and control loads necessary to maintain hardware functionality and prevent damage in extreme cold conditions. As such, the values presented here reflect realistic operational energy demands for a PSR deployment, rather than an isolated subsystem efficiency. These values do not, however, include the energy needs for excavation and handling. The reported recovery and extraction rates include extended steady-state periods (e.g., overnight operation) during which the system was intentionally held at stable

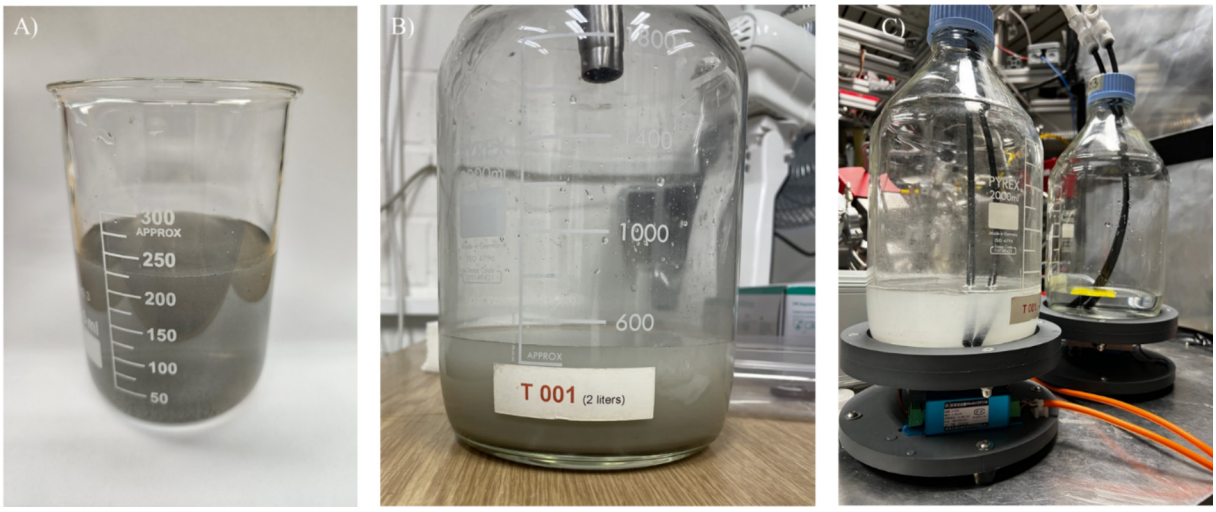

Fig. 10. Recovered water from several experiments. A) After Experiment 1, B) after Experiment 4, and C) shows the recovered water as it is being purified.

Table 7
Experimental performance metrics results.

Experiment	1	2	3	4
Total Active Time (h)	54.79	140.00	123.94	230.22
Total Energy Used (kWh)	5.73	16.39	15.52	20.72
Average Total Heater Power (W)	104.58	117.07	125.22	90.00
Total Extraction Time (h)	20.51	93.03	96.14	118.54
WES Energy Used (kWh)	2.93	6.99	7.67	10.49
Average WES Heater Power (W)	142.86	75.14	79.78	88.49
Ice Mass summed (g)	442	1687	948	653
Recovered Water Mass (g)	255	1087	509	474
Recovery Percentage (%)	58%	64%	54%	73%
Recovery Rate (g/h)	4.65	7.76	4.11	2.06
Residual Ice Mass (g)	–*	138	13	119
Extracted Water Mass (g)	–†	1549	935	534
Extraction Percentage (%)	–†	92%	99%	82%
Extraction Rate (g/h)	–†	16.65	9.73	4.50
Capture Percentage (%)	–†	70%	54%	89%
Loss Mass (g)	–†	462	426	60
Extraction Energy Efficiency (g/kWh)	–†	221.49	121.88	50.91
Recovery Energy Efficiency (g/kWh)	44.51	66.33	32.80	22.88

* The residual ice mass after the experiment was not measured for Experiment 1.
† Could not be calculated because the residual ice mass was not measured.

conditions. Consequently, the calculated rates represent conservative, campaign-level averages and could be increased by reducing non-productive hold time through operational optimisation. The inclusion of these periods also increases total energy consumption, since heater power is continuously required to maintain operational temperatures over extended durations.

4.3. Qualitative observations

Besides the quantitative results, some observations during the experiments have led to qualitative results. Specifically, observations from the cameras yielded interesting results on the effect of contamination on water capturing and on the optimal concept of operations.

4.3.1. Ice accretion and delamination behaviour

Ice deposition on the cold finger was consistently tracked through video monitoring, enabling quantitative analysis of ice accretion rates in post-processing (Fig. 11). The delamination phase had varied success across experiments. In most cases, ice did not release as cleanly as intended but instead underwent partial sublimation before detaching in fragmented pieces. Sublimated vapour was subsequently re-deposited onto colder surfaces inside the liquefaction chamber, which were then deliberately used as a secondary cold trap by not heating the liquefaction chamber walls. This unintended effect complicated final water recovery and may have contributed to variations observed in overall capturing efficiencies.

4.3.2. Methanol contamination effects

The introduction of methanol contamination in Experiment 3 significantly impacted ice deposition and capturing effectiveness. Unlike other tests, a liquid (most likely pure methanol) visibly condensed onto the cold finger surfaces at a certain point during the experiment, as can be seen in Fig. 12, a phenomenon not observed in methanol-free experiments. The presence of liquid methanol appeared to inhibit effective deposition of water ice, directly correlating with substantially lower capturing and consequently overall recovery efficiencies. Pressure and temperature logs suggest the cold finger operated near the narrow pressure–temperature range, allowing liquid-phase methanol formation, indirectly informing the actual surface temperatures of the cold fingers during the capturing process, as reconstructed in Fig. 13. This figure was created using multiple sources (Ambrose and Walton, 1989; Linstrom, 1997; Murphy and Koop, 2005; Wagner and Pruß, 2002). The pressures shown in the figure relate to the LUWEX internal process volumes, and not the pressure on the surface of the Moon.

4.3.3. Stirring impact

In Experiment 3, the stirring mechanism was activated partway through the extraction phase to assess its influence on system performance. Stirring was initiated after several hours, once power consumption and chamber pressure had decreased to relatively steady values, indicating reduced sublimation activity. It was then operated until no more sublimation activity was observed, through visually confirming that no more ice was accreting.

Following the start of stirring, a small but distinct increase in heater power consumption was observed, suggesting improved heat dissipation from the extraction subsystem. The magnitude of this effect varied between tests and remained modest. A much more pronounced effect was seen in the chamber pressure, which rose by nearly an order of magnitude within minutes of stirring, as can be seen in Fig. 14. This is likely due to the movement of hot simulant material near the heaters into contact with colder, ice-rich regions, causing rapid localised sublima-

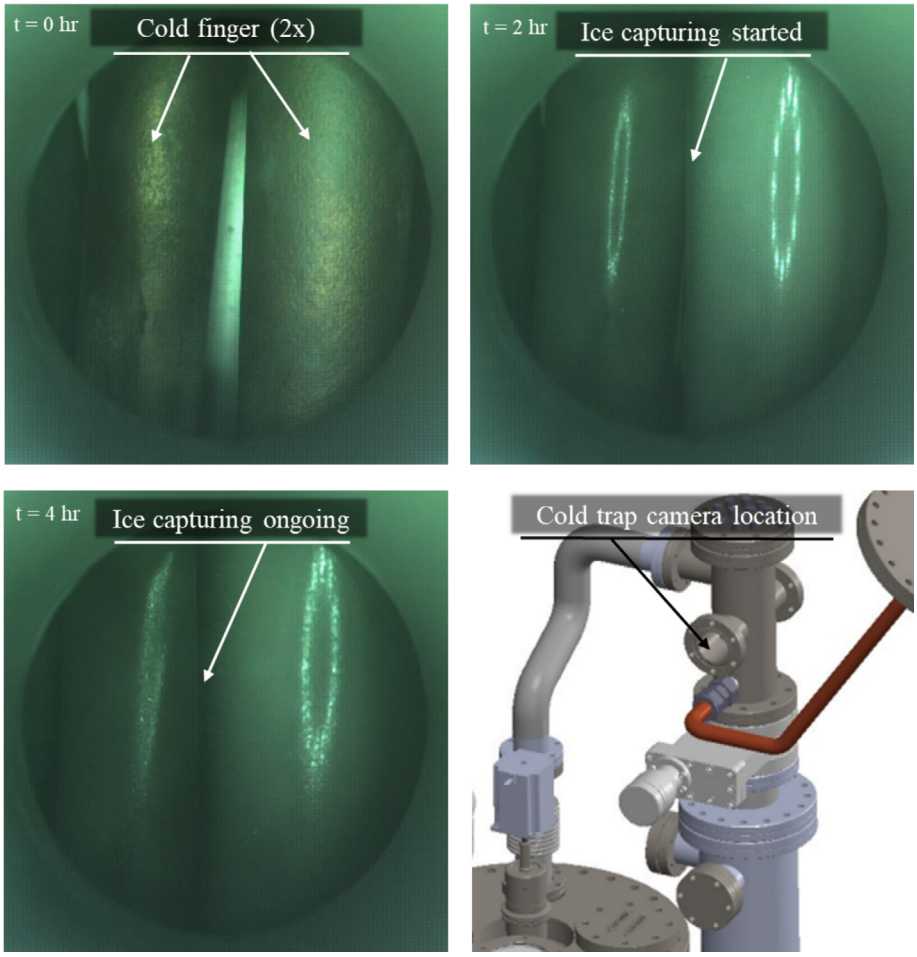

Fig. 11. Images from the copper cold fingers seen through the cold trap viewing port of Experiment 2.0 at t = 0 h, t = 2 h, and t = 4 h, where the captured ice is visibly accreting sideways. The cold fingers are conically shaped and internally cooled with LN_2. Additionally, the location of the camera is shown.

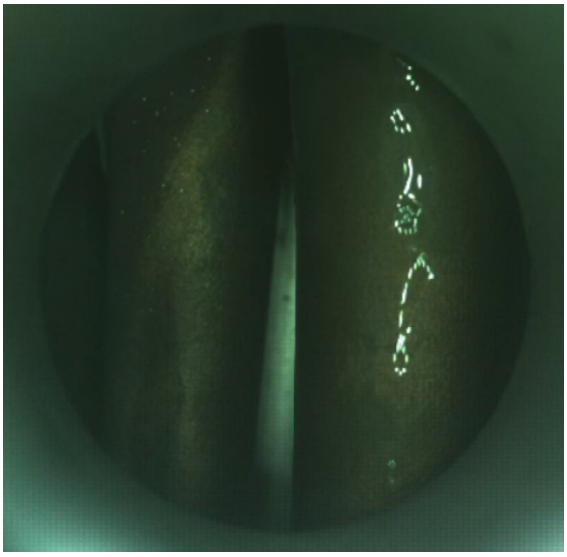

Fig. 12. Liquid methanol is visibly condensing on the cold fingers.

tion. In tests where heaters were not powered at the time of stirring onset, this pressure increase was delayed until heating resumed.

Despite the marked change in pressure, no corresponding increase in ice thickness accretion on the cold trap was detected. This indicates that the capturing subsystem was already operating at its maximum effective capturing rate before stirring began, and that any additional vapour released could not be deposited and was instead lost to pumping. This supports other indications within the results that the cold trap is a bottleneck in the current configuration.

5. Discussion and future work

5.1. Interpretation of results

Two unexpected observations emerged from the LUWEX experiments. First, dust mobilisation proved more severe than anticipated. Although dust-related chal-

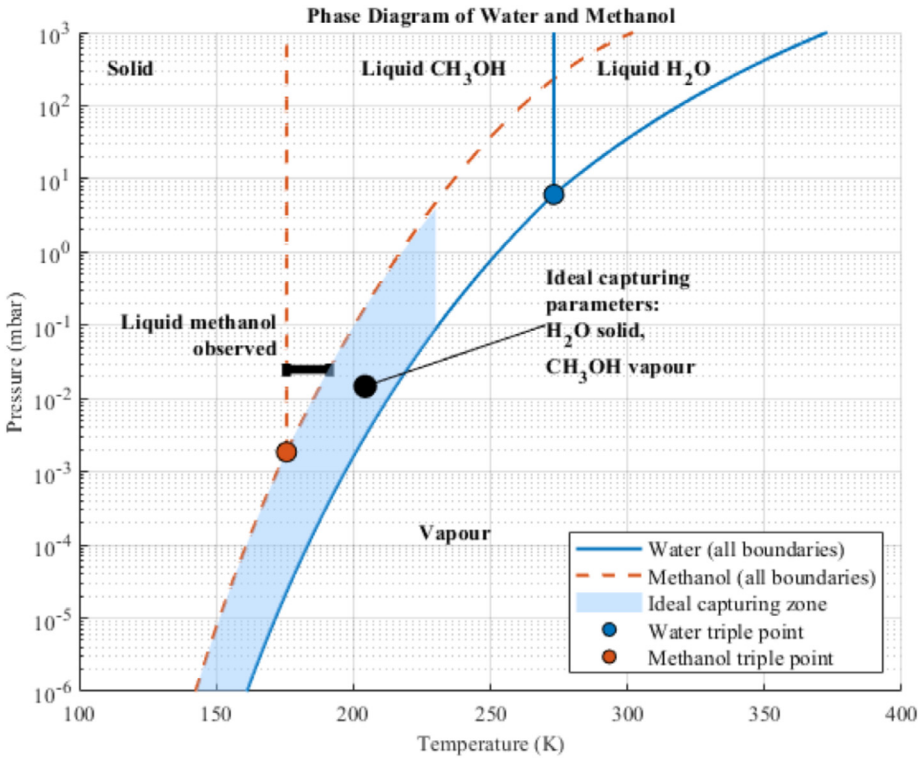

Fig. 13. Phase diagram including triple points of water and methanol, with the pressure at which liquid methanol was observed and its resulting possible temperature range. The ideal internal capturing parameters for water are marked between the water–ice boundary and the methanol-vapour boundary.

lenges are well known in lunar surface operations, the number of airborne particles in these tests was higher than expected. The circulating dust quickly obscured camera views, as can be seen in Fig. 15, and interfered with hardware seals, most notably the pneumatic slider in the capturing subsystem. Dust infiltration prevented this valve from sealing properly, which in turn hampered the liquefaction phase by allowing water vapour to leak instead of being fully retained. To continue operations despite this issue, the team adopted a strategy of performing multiple extraction–capture cycles before a final liquefaction step at the end of each run. This workaround enabled the completion of experiments but may have introduced variability in the icy regolith structure due to repeated refilling. Overall, the dust behaviour observed underlines the need for robust dust mitigation measures in future lunar ISRU designs. When vapour generation outpaced capture, the resulting rise in internal pressure likely made particles become airborne more readily, which is consistent with the observed dust mobilisation and corresponding pressures. Ongoing analyses will examine the sizes and distribution of the airborne dust particles and correlate them with chamber pressure conditions to better understand and manage this phenomenon.

Second, tests involving methanol contamination produced an unanticipated outcome, where liquid methanol condensed on the cold finger surfaces. Under the expected temperature and pressure conditions, methanol was presumed to remain gaseous and not co-deposit with water. In practice, however, the methanol vapour condensed, forming a liquid film that likely impeded water ice deposition and significantly reduced the efficiency of vapour capture. The original intent had been to leverage the cold trap as a crude purification step by trapping water while leaving contaminants like methanol in the gas phase. The experimental results indicate that this selective trapping approach is difficult to achieve without precise thermal control, since the cold finger temperature could not be finely regulated to discriminate between water and methanol condensation. These findings suggest that future systems must either implement tighter temperature control for cold-trapping or explore alternative capture designs to handle mixed volatiles. Improved thermal regulation or multi-stage trapping could help ensure that contaminants do not degrade water capture performance in an operational lunar environment.

5.2. Experiment improvement opportunities

The experiments faced several known boundaries regarding instrumentation and thermal management. Sensor placement was limited and resulted in incomplete thermal data, especially concerning the actual cold finger surface temperatures and sample temperature in the crucible. This limited sensor coverage made precise control and assessment of thermal conditions challenging. To address this, future analyses shall explore the relationship between observed pressures and measured ice accretion

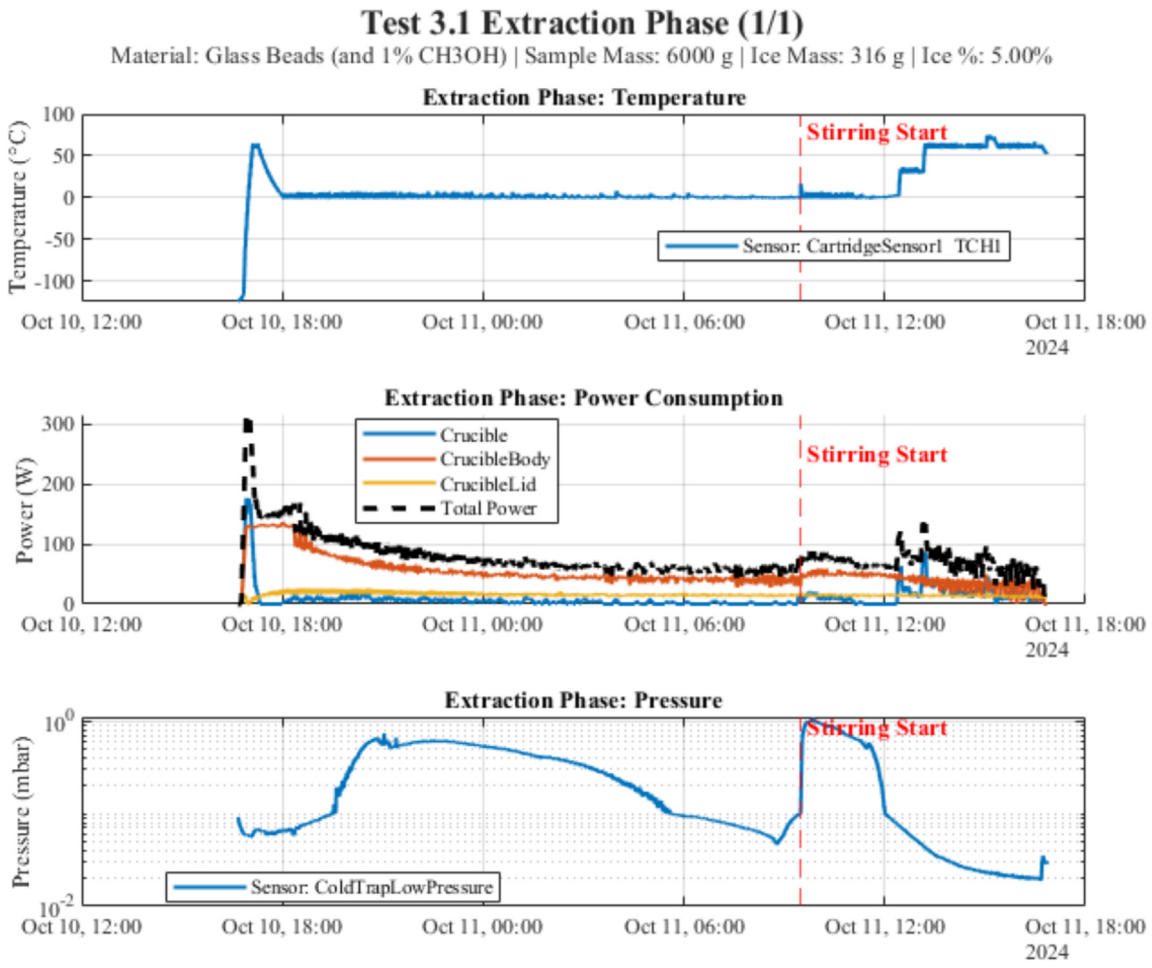

Fig. 14. Stirring impact measured across temperature, power, and pressure.

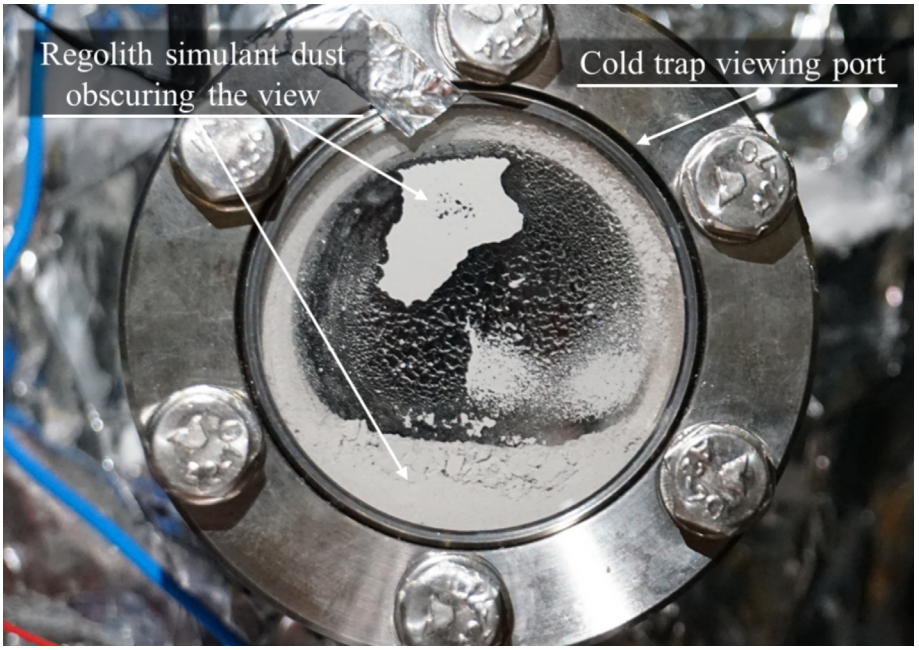

Fig. 15. Regolith simulant dust (light grey) that accumulated in the cold trap viewing port during the final capturing phase of Experiment 4.0.

rates more comprehensively, aiming to clarify inefficiencies in vapour capturing. Future integrated analysis of visual ice accretion data and pressure excursions will better quantify capturing losses and support optimisation of operational parameters in future hardware iterations.

The cold fingers were actively cooled from the inside to approximately –170 °C using circulating liquid nitrogen. This approach was practical for ground testing but is not representative of a lunar deployment, where such cooling would need to be achieved through space-qualified cryocoolers or by radiative cooling to deep space. Consequently, while the present results reflect the thermal performance achievable under LN_2 cooling, they may overestimate capturing efficiency compared to a fully flight-representative system. Similarly, thermal control limitations were particularly pronounced during the delamination phase. The heating wires used to warm the cold finger surfaces did not deliver sufficient heat rapidly enough to effectively detach deposited ice. This issue arose from inherently low thermal conduction in vacuum conditions, emphasising the need for enhanced thermal interfaces or alternative delamination techniques, such as mechanical vibration or optimised heating and capturing strategies.

The choice of glass beads as a simulant in some experiments was a practical decision made to mitigate early dust issues rather than a design choice aimed at replicating lunar regolith characteristics closely. Consequently, some thermal and mechanical behaviours (e.g. heat distribution and particle interaction) might differ from those with a realistic lunar regolith simulant. Future tests should revisit the use of more representative lunar simulants, assuming dust mitigation solutions (active or passive) can be successfully implemented.

Data logging frequency (1 Hz) introduced uncertainties, particularly in the measurement of power consumption. Short-duration heater activation (on the order of a few seconds) risked being underrepresented, leading to potential inaccuracies in calculated energy metrics. Additionally, pressure sensor readings primarily indicated system equilibrium states between the pumps and the sublimation rate, rather than precise localised pressure values.

Finally, the procedure of periodic sample refilling (to maintain roughly 5% ice by mass throughout) could have led to an uneven ice distribution in the crucible over time, even though stirring could have limited this effect. The upper layers of regolith would be refreshed with new ice, while lower layers became progressively drier, potentially affecting extraction rates and overall consistency. All experiments were carried out with the same refilling method, which provides a consistent basis for comparison. However, this practice introduces uncertainty about how uniform the ice content was during each extraction cycle. Recognising these limitations is important for interpreting the LUWEX results and for guiding improvements in follow-up experiments and prototype development.

5.3. Future challenges of lunar water extraction

The outcomes of the LUWEX project demonstrate that end-to-end thermal extraction, vapour capture, and water collection are technically feasible, while also clarifying the challenges that future lunar ISRU systems must overcome. A key insight is that non-water volatiles present in the regolith can significantly impede the capture process. The experiments showed that contaminants like methanol in the vapour stream can reduce the efficiency of water collection by condensing or otherwise interfering with ice deposition. This finding highlights the need for a dedicated contamination management strategy. In practice, lunar water extraction systems should be designed either to operate under conditions that minimise the co-capture of undesirable volatiles or to include mechanisms (such as phased capturing steps or sorbents) that separate and handle impurities. Any chosen strategy will require validation to ensure that high water recovery rates can be maintained even when the feed material contains a mix of volatile substances.

Another challenge lies in scaling the extraction and capture subsystems in accordance with each other. Simply increasing the heating power or the throughput of an extraction unit will not yield more recovered water unless the capture capacity is enlarged in tandem. The LUWEX tests indicate that the extraction and capture processes must be treated as a tightly coupled system, since whenever the extraction rate exceeds the capture capacity, the internal pressure rises and dust particles become airborne more readily, leading to losses and operational degradation. Future designs should ensure that for any given extraction rate, the cold trap or condenser can accommodate that vapour flow without significant losses. In other words, the capture subsystem should always slightly outpace the extraction subsystem so that additional heat input translates into greater liquid yield rather than increased potential bypass losses. This systems-level approach to sizing and operating the hardware will be critical in maximising the efficiency of a lunar water extraction plant.

Reliable transfer of captured ice to storage is also an area requiring attention. In the LUWEX setup, the ice delamination step (releasing ice from the cold finger for melting) did not always perform consistently. In a future lunar unit, any uncertainty or delay in moving collected ice into a melt reservoir could reduce overall throughput and complicate mass accounting. To address this, engineers could pursue more robust delamination mechanisms, such as faster or more uniform heating of the cold surfaces, mechanical scrapers, or vibration-assisted removal. Alternatively, operational approaches might be adjusted, for instance, using multiple cold traps that alternate between capturing and melting phases, to ensure a smooth, continuous transfer of ice to liquid water. The overarching requirement is a predictable and repeatable method for clearing the capture surface so that each cycle of operation

can begin fresh without lingering ice impeding performance.

Dust mitigation will remain an ever-present challenge for lunar surface operations, and LUWEX reinforced its significance. Dust particles affected moving seals and interfaces in the experiment, leading to performance degradation over time. Although dust did not halt the system's operation outright, it introduced extra maintenance steps and uncertainties. Future extraction system designs should proactively minimise the exposure of sensitive components to the regolith and dust-laden vapours. This can be achieved by simplifying and sealing interfaces where possible, using geometry and materials that are less prone to dust accumulation, and incorporating shields or filters to protect critical moving parts. In extreme cases, active dust-clearing techniques (like gas blow-off or electrostatic dust removal) could be employed at key points to ensure long-term reliability. Addressing dust is not a singular technical hurdle but rather an ongoing engineering consideration, one that must be integrated into the design philosophy of lunar ISRU hardware.

Finally, the scalability and architecture of the water extraction system should be guided by the insights from LUWEX. Certain design elements that worked at the laboratory scale may not translate directly to a larger, mission-scale system. For example, the mechanical stirring used to enhance heat transfer in the LUWEX crucible was effective for ~10 kg batches, but implementing a similar approach for substantially larger volumes could be complex or impractical. Likewise, the cold finger-based capture method, while successful in these tests, inherently faces limits due to the slow heat transfer in a vacuum. A much larger cold trap would be needed for higher processing rates, or else the capture process might become a throughput bottleneck. Future systems should consider modular or parallel configurations, such as multiple smaller extraction units feeding multiple cold traps or condensers, to allow throughput to scale up without hitting single-point limitations. Design options like alternating two cold traps (so one is capturing vapour while the other melts collected ice, also rendering delamination redundant) could increase continuous output and avoid downtime. The trade-offs between complexity, reliability, and efficiency will need careful evaluation, but the core lesson is that both extraction and capture processes must grow together in capacity. The LUWEX project, having achieved an integrated demonstration at relevant conditions, provides a valuable stepping stone towards higher-TRL lunar water ISRU systems.

5.4. Mission Scenario Examples

Using the recovery rates from Table 7, the demonstrated recovered-water throughput corresponds to an equivalent continuous production of approximately 0.05–0.19 kg/day (based on 2.06–7.76 g/h). For context, ISS crew water use is on the order of 1 gallon (~3.8 kg) per crewmember per day for drinking, food preparation, and hygiene (Ewert et al., 2022), while current ISS water processing can achieve ~98% water recovery (Schneider and Shull, 2017), implying a make-up demand of ~0.08 kg/crew-day if a comparable closed-loop system is available. Under the simplifying assumption that excavation, transport, downstream purification, and electrolysis (for propellant) are not rate-limiting, the best demonstrated LUWEX throughput would therefore cover make-up water for ~2–3 crew members, or about 5% of the daily demand per person without recycling. In terms of propellant production, electrolysis conserves mass such that 1 kg H_2O yields 1 kg of $O_2 + H_2$ (neglecting processing losses). An Apollo-like lunar ascent to a 110 km orbit required on the order of 2377 kg of propellant (Orloff and Garber, 2000), suggesting ~35 LUWEX units operating continuously for one year at the best demonstrated recovered-water throughput (ignoring specifics such as fuel type, specific impulse and delta V). Using a realistic fuel-rich oxygen-to-hydrogen mixture ratio of about 6, hydrogen becomes limiting, and about 1.29 kg of water must be electrolysed per kilogram of propellant. This is because splitting water produces significantly more oxygen than hydrogen by mass (following its stoichiometric ratio), while a fuel-rich engine still requires a relatively large fraction of hydrogen. Therefore, additional water must be processed to generate enough hydrogen, resulting in excess oxygen. This increases the required water for an Apollo-like ascent to ~3056 kg and the corresponding scaling to ~45 LUWEX units operating continuously for one year. These comparisons are intended as order-of-magnitude context only. The reported rates include periods of steady-state operation (e.g., overnight holds) and are expected to improve with operational optimisation, increased capture capacity, and parallelisation. Ultimately, for such mission scenarios, a specific water extraction design should be developed.

6. Conclusions

The LUWEX experimental campaign successfully validated a fully integrated lunar water extraction, capture, and liquefaction process at a scale and fidelity beyond most prior studies, processing up to 13 kg of icy simulant per run under PSR-like conditions. Across several test configurations, the system consistently sublimated and recovered a substantial fraction of the water from icy simulants, confirming the technical feasibility of end-to-end thermal extraction from a crucible (with stirring capability), cold-trap capture, and liquefaction in a DTVAC with cryogenic cold shrouds. Major findings include the importance of balancing the extraction rate with capture capacity. Tests showed that simply increasing heating power does not translate to higher liquid yields unless the capturing system can accommodate the additional vapour. The experiments also revealed operational challenges, notably the severe mobilisation of dust and the condensation of non-water volatiles, both of which can impair hardware performance

by degrading seals and reducing capture efficiency via liquid films on cold trapping surfaces. Across campaigns, total water recovery ranged ~50–70% (peaking near ~73%) with capture efficiencies approaching ~90% in the best runs. Regarding recovery energy efficiency, values of up to 66.33 g/kWh were reached for the icy glass beads simulants whilst stirring, and 22.88 g/kWh for the icy regolith simulant experiments without stirring. These numbers reflect the total energy demand for water recovery and maintaining operational temperatures in a PSR.

Taken together, these results provide a proof of concept for scaled and integrated ISRU operations and point to concrete design priorities: dust-resistant mechanisms and procedures, greater vapour-capture capacity (e.g., increased area or staged traps) to match peak sublimation, and contaminant-aware thermal control of the capturing surfaces. These results offer valuable empirical data and experience to guide the development of robust lunar ISRU water systems.

CRediT authorship contribution statement

Luca Kiewiet: Conceptualization, Methodology, Investigation, Formal analysis, Data curation, Visualization, Writing – original draft, Writing – review & editing, Funding acquisition. **Svenja Fälker:** Methodology, Visualization, Writing – review & editing. **Mateo Rejón López:** Methodology, Visualization, Writing – review & editing. **Paul Zabel:** Conceptualization, Methodology, Writing – review & editing, Supervision, Project administration, Funding acquisition.

Funding

This work was conducted in the context of the project LUWEX, which is funded by the European Union under grant agreement no. 101081937 – Horizon 2022 – Space Science and Exploration Technologies. Views and opinions expressed are, however, those of the authors only and do not necessarily reflect those of the European Union; neither the European Union nor the granting authority can be held responsible for them.

Declaration of competing interest

The authors declare the following financial interests/personal relationships which may be considered as potential competing interests: Luca Kiewiet reports financial support was provided by European Union. If there are other authors, they declare that they have no known competing financial interests or personal relationships that could have appeared to influence the work reported in this paper.

Acknowledgements

We thank the CoPhyLab/TU Braunschweig team for operating support and access to the DTVAC facility. We also acknowledge the LUWEX consortium partners for their technical discussions and assistance during the design, assembly, integration, and testing phases. Special thanks to Angel Abbud-Madrid and Julie Brisset for their feedback as external advisors of the LUWEX project.

Data availability

The datasets generated and analysed during the current study are available from the corresponding author on request.

References

Ambrose, D., Walton, J., 1989. Vapour pressures up to their critical temperatures of normal alkanes and 1-alkanols. Pure Appl. Chem. 61 (8), 1395–1403. https://doi.org/10.1351/pac198961081395.

Boscheri, G., Marchitelli, G., Fili, T., Perelli, R., Zabel, P., Rejón López, M., 2025. Laboratory validation of the water purification subsystem for lunar in-situ resource utilization in the LUWEX project. 54th International Conference on Environmental Systems.

Clark, R.N., 2009. Detection of adsorbed water and hydroxyl on the Moon. Science (New York, N.Y.) 326 (5952), 562–564. https://doi.org/10.1126/science.1178105.

Colaprete, A., Schultz, P., Heldmann, J., Wooden, D., Shirley, M., Ennico, K., Hermalyn, B., Marshall, W., Ricco, A., Elphic, R.C., Goldstein, D., Summy, D., Bart, G.D., Asphaug, E., Korycansky, D., Landis, D., Sollitt, L., 2010. Detection of water in the LCROSS ejecta plume. Science (New York, N.Y.) 330 (6003), 463–468. https://doi.org/10.1126/science.1186986.

Elphic, R.C., Eke, V.R., Teodoro, L.F.A., Lawrence, D.J., Bussey, D.B.J., 2007. Models of the distribution and abundance of hydrogen at the lunar south pole. Geophys. Res. Lett. 34 (13). https://doi.org/10.1029/2007GL029954 2007GL029954.

Ewert, M.K., Chen, T.T., Powell, C.D., 2022. Life Support Baseline Values and Assumptions Document (NASA/TP-2015-218570/REV2). National Aeronautics and Space Administration (NASA).

Feldman, W.C., Maurice, S., Binder, A.B., Barraclough, B.L., Elphic, R. C., Lawrence, D.J., 1998. Fluxes of fast and epithermal neutrons from Lunar Prospector: evidence for water ice at the lunar poles. Science (New York, N.Y.) 281 (5382), 1496–1500. https://doi.org/10.1126/science.281.5382.1496.

Gladstone, G.R., Hurley, D.M., Retherford, K.D., Feldman, P.D., Pryor, W.R., Chaufray, J.-Y., Versteeg, M.H., Greathouse, T.K., Steffl, A.J., Throop, H., Parker, J.W., Kaufmann, D.E., Egan, A.F., Davis, M.W., Slater, D.C., Mukherjee, J., Miles, P.F., Hendrix, A.R., Colaprete, A., Stern, S.A., 2010. LRO-LAMP observations of the LCROSS impact plume. Science (New York, N.Y.) 330 (6003), 472–476. https://doi.org/10.1126/science.1186474.

Gladstone, G.R., Retherford, K.D., Egan, A.F., Kaufmann, D.E., Miles, P.F., Parker, J.W., Horvath, D., Rojas, P.M., Versteeg, M.H., Davis, M.W., Greathouse, T.K., Slater, D.C., Mukherjee, J., Steffl, A.J., Feldman, P.D., Hurley, D.M., Pryor, W.R., Hendrix, A.R., Mazarico, E., Stern, S.A., 2012. Far-ultraviolet reflectance properties of the Moon's permanently shadowed regions. J. Geophys. Rese. Planets 117 (E12). https://doi.org/10.1029/2011JE003913 2011JE003913.

Hayne, P.O., Aharonson, O., Schörghofer, N., 2021. Micro cold traps on the Moon. Nat. Astron. 5 (2), 169–175. https://doi.org/10.1038/s41550-020-1198-9.

Hayne, P.O., Hendrix, A.R., Sefton-Nash, E., Siegler, M.A., Lucey, P.G., Retherford, K.D., Williams, J.-P., Greenhagen, B.T., Paige, D.A., 2015. Evidence for exposed water ice in the Moon's south polar regions from Lunar Reconnaissance Orbiter ultraviolet albedo and temperature measurements. Icarus 255, 58–69. https://doi.org/10.1016/j.icarus.2015.03.032.

Holquist, J.B., Gellenbeck, S., Bower, C.E., Tewes, P., 2021. Experimental proof of concept of a cold trap as a purification step for lunar water processing. 50th International Conference on Environmental Systems.

Holquist, J.B., Pasadilla, P., Bower, C.E., Cognata, T., Tewes, P., Kelsey, L., 2020. Analysis of a cold trap as a purification step for lunar water processing. In: 49th International Conference on Environmental Systems (ICES-2020-71), pp. 1–12.

Ikeya, K., Guerrero-Gonzalez, F.J., Kiewiet, L., Cardin, M.-A., Cilliers, J.J., Starr, S., Hadler, K., 2025. Hybrid lunar ISRU plant: a comparative analysis with carbothermal reduction and water extraction. Acta Astronaut. 230, 148–168. https://doi.org/10.1016/j.actaastro.2025.02.004.

Imhof, B., Brandić Lipińska, M., Waclavicek, R., Retat, I., Zabel, P., Blum, J., Boscheri, G., Leluk, K., Kiewiet, L., Heitkamp, M., Wache, H., Rejón López, M., Kreuzig, C., Meier, G., Noria Brecher, J., Bürger, J., Perelli, R., Marchitelli, G., Maida, F., Sidorowicz, M., 2024. LUWEX: validation of lunar water extraction and purification technologies for in-situ propellant and consumables production. 75th International Astronautical Congress (IAC).

Jurado, N.I., Amato, A.D., Mendoza, P.A., Negron-Ortiz, E., Torres, I. A., Amador, A., Rahman, M.M., Greig, A.D., Choudhuri, A., 2021. Increasing ice collection rates on engineered cold plate under cryogenic vacuum conditions. In: ASCEND 2021. https://doi.org/10.2514/6.2021-4045.

Kiewiet, L., Fälker, S., Zabel, P., 2025. A review of lunar water extraction technologies: comparison, classification, and research gaps. Space Planet. Resour. 1 (1). https://doi.org/10.1007/s44461-025-00005-4.

Kleinhenz, J.E., Paz, A., 2020. Case studies for lunar ISRU systems utilizing polar water. In: ASCEND 2020. American Institute of Aeronautics and Astronautics. https://doi.org/10.2514/6.2020-4042.

Kornuta, D., Abbud-Madrid, A., Atkinson, J., Barr, J., Barnhard, G., Bienhoff, D., Blair, B., Clark, V., Cyrus, J., DeWitt, B., Dreyer, C.B., Finger, B., Goff, J., Ho, K., Kelsey, L., Keravala, J., Kutter, B., Metzger, P.T., Montgomery, L., Zhu, G., 2019. Commercial lunar propellant architecture: a collaborative study of lunar propellant production. Reach 13. https://doi.org/10.1016/j.reach.2019.100026 100026.

Kreuzig, C., Bischoff, D., Molinski, N.S., Brecher, J.N., Kovalev, A., Meier, G., Oesert, J., Gorb, S.N., Gundlach, B., Blum, J., 2023. Micrometre-sized ice particles for planetary science experiments – CoPhyLab cryogenic granular sample production and storage. RAS Tech. Instrum. 2 (1), 686–694. https://doi.org/10.1093/rasti/rzad049.

Kreuzig, C., Kargl, G., Pommerol, A., Knollenberg, J., Lethuillier, A., Molinski, N.S., Gilke, T., Bischoff, D., Feller, C., Kührt, E., Sierks, H., Hänni, N., Capelo, H., Güttler, C., Haack, D., Otto, K., Kaufmann, E., Schweighart, M., Macher, W., Tiefenbacher, P., Gundlach, B., Blum, J., 2021. The CoPhyLab comet-simulation chamber. Rev. Sci. Instrum. 92 (11). https://doi.org/10.1063/5.0057030 115102.

Li, S., Lucey, P.G., Milliken, R.E., Hayne, P.O., Fisher, E., Williams, J.-P., Hurley, D.M., Elphic, R.C., 2018. Direct evidence of surface exposed water ice in the lunar polar regions. Proc. Natl. Acad. Sci. U. S.A. 115 (36), 8907–8912. https://doi.org/10.1073/pnas.1802345115.

Linke, S., Windisch, L., Kueter, N., Wanvik, J.E., Voss, A., Stoll, E., Schilde, C., Kwade, A., 2020. TUBS-M and TUBS-T based modular Regolith Simulant System for the support of lunar ISRU activities. Planet. Space Sci. 180. https://doi.org/10.1016/j.pss.2019.104747 104747.

Linstrom, P., 1997. Nist Chemistry WebBook, NIST Standard Reference Database 69.

Lunex Technologies GmbH, 2024. 75% Terrae – 25% Mare Lunar Regolith Simulant Datasheet v1.

Murphy, D.M., Koop, T., 2005. Review of the vapour pressures of ice and supercooled water for atmospheric applications. Q. J. R. Meteorolog. Soc. 131 (608), 1539–1565. https://doi.org/10.1256/qj.04.94.

National Aeronautics and Space Administration (NASA), 2021. Classifications and Requirements for Testing Systems and Hardware to be Exposed to Dust in Planetary Environments (Technical Standard NASA-STD-1008). https://standards.nasa.gov/sites/default/files/standards/NASA/Baseline/0/2021-08-21_nasa-std-1008-approved.pdf.

Orloff, R.W., Garber, S., 2000. Apollo by the Numbers: A Statistical Reference (NASA/SP-2000-4029). National Aeronautics and Space Administration (NASA).

Patzwald, J., Kleba-Ehrhardt, R., Griemsmann, T., Nowaczyk, N., Linke, S., Overmeyer, L., Stoll, E., Karl, D., 2025a. Properties of novel LX lunar regolith simulant system — the base simulants: part 2. Planet. Space Sci. 268. https://doi.org/10.1016/j.pss.2025.106189 106189.

Patzwald, J., Kleba-Ehrhardt, R., Schiperski, F., Griemsmann, T., Linke, S., Neumann, T., Overmeyer, L., Stoll, E., Karl, D., 2025b. Properties of novel LX lunar regolith simulant system — the base simulants: part 1. Acta Astronaut. 231, 200–222. https://doi.org/10.1016/j.actaastro.2025.02.030.

Pieters, C.M., Goswami, J.N., Clark, R.N., Annadurai, M., Boardman, J., Buratti, B., Combe, J.-P., Dyar, M.D., Green, R., Head, J.W., Hibbitts, C., Hicks, M., Isaacson, P., Klima, R., Kramer, G., Kumar, S., Livo, E., Lundeen, S., Malaret, E., Varanasi, P., 2009. Character and spatial distribution of OH/H_2O on the surface of the Moon seen by M3 on Chandrayaan-1. Science (New York, N.Y.) 326 (5952), 568–572. https://doi.org/10.1126/science.1178658.

Purrington, C.A., Purcell, D., Schmit, J., Thrift, B., 2023. Rapid extraction of volatiles from excavated icy regolith using a rotary extraction drum. In: Dreyer, C.B., Littell, J. (Eds.), Earth and Space 2022. American Society of Civil Engineers, pp. 363–373. https://doi.org/10.1061/9780784484470.034.

Reiss, P., 2024. Exploring the lunar water cycle. Proc. Natl. Acad. Sci. U. S.A. 121 (52). https://doi.org/10.1073/pnas.2321065121 e2321065121.

Reiss, P., Grill, L., Barber, S.J., 2019. Thermal extraction of volatiles from the lunar regolith simulant NU-LHT-2M: Preparations for in-situ analyses on the Moon. Planet. Space Sci. 175, 41–51. https://doi.org/10.1016/j.pss.2019.05.001.

Sanin, A.B., Mitrofanov, I.G., Litvak, M.L., Bakhtin, B.N., Bodnarik, J. G., Boynton, W.V., Chin, G., Evans, L.G., Harshman, K., Fedosov, F., Golovin, D.V., Kozyrev, A.S., Livengood, T.A., Malakhov, A.V., McClanahan, T.P., Mokrousov, M.I., Starr, R.D., Sagdeev, R.Z., Tret'yakov, V.I., Vostrukhin, A.A., 2017. Hydrogen distribution in the lunar polar regions. Icarus 283, 20–30. https://doi.org/10.1016/j.icarus.2016.06.002.

Schneider, W., Shull, S.A., 2017. NASA advanced explorations systems: 2017 advancements in life support systems. In: AIAA SPACE and Astronautics Forum and Exposition. American Institute of Aeronautics and Astronautics. https://doi.org/10.2514/6.2017-5152.

Sigmund Lindner GmbH, 2018. Product Data Sheet SiLibeads Glass beads Type S. https://www.sili.eu/wp-content/uploads/2018/08/SiLibeads_Type_S-1.pdf.

Sunshine, J.M., Farnham, T.L., Feaga, L.M., Groussin, O., Merlin, F., Milliken, R.E., A'Hearn, M.F., 2009. Temporal and spatial variability of lunar hydration as observed by the deep impact spacecraft. Science (New York, N.Y.) 326 (5952), 565–568. https://doi.org/10.1126/science.1179788.

Wache, H., Kiewiet, L., Zabel, P., Blum, J., 2025. Investigation of the thermal conductivity of dry and icy lunar regolith simulants. J. Geophys. Res. Planets 130 (9). https://doi.org/10.1029/2025JE009084 e2025JE009084.

Wagner, W., Pruß, A., 2002. The IAPWS formulation 1995 for the thermodynamic properties of ordinary water substance for general and scientific use. J. Phys. Chem. Ref. Data 31 (2), 387–535. https://doi.org/10.1063/1.1461829.